Ocean Modelling 197 (2025) 102590

Contents lists available at ScienceDirect

Ocean Modelling

journal homepage: www.elsevier.com/locate/ocemod

Impact of sea ice friction on ocean tides in the Arctic Ocean, modelling insights at various time and space scales

Mathilde Cancet[a], Florent H. Lyard[b], Ergane Fouchet[a,*]

[a] NOVELTIS S.A.S., Labège, 31670, France
[b] LEGOS, Université de Toulouse, CNES, CNRS, IRD, Toulouse, 31400, France

ARTICLE INFO

Keywords:
Arctic ocean
Tidal modelling
Sea ice cover
Climate change

ABSTRACT

Although ocean tides are one of the major contributors to the energy dissipation in the Arctic Ocean, they remain relatively poorly known, particularly their interactions with the ice cover (sea ice and grounded ice). These interactions are often simply ignored in tidal models, or considered through relatively simple combinations with the bottom friction. In this paper, we investigate the response of a regional pan-Arctic ocean tidal model to the friction under the sea ice cover, in order to better understand the influence of this parameter on tidal estimates. Different periods of time, from seasonal to decadal scales, were considered to analyze the impact of the variations in the sea ice cover on the ocean tides, in the region as well as at global scale. Long-distance effects of Arctic sea ice friction are revealed in the global tidal simulations, resulting in variations of several centimeters in the seasonal tidal amplitudes. Tide gauge and satellite altimetry observations were specifically processed to retrieve the tidal harmonic constituents over different periods and different sea ice conditions, to compare with the model simulations. Improving the knowledge on the interaction between the tides and the sea ice cover, and thus the performance of the tidal models in the polar regions, is of particular interest to generate more realistic simulations with ocean circulation models, to contribute to scientific investigations on the changes in the Arctic Ocean, and also to improve the satellite altimetry observation retrievals at high latitudes, as the tidal signals remain a major contributor to the error budget of the satellite altimetry observations in the Arctic Ocean. This work also highlights the difficulty to assess the temporal evolution of tides in model simulations in the Arctic because of the lack of long (i.e. several decades) hourly tide gauge observation records in the area.

1. Introduction

The ocean tides are one of the major contributors to the energy dissipation in the Arctic Ocean (Rippeth et al., 2015). In particular, barotropic tides are quite sensitive to friction processes, and thus to the presence of sea ice in polar regions, as friction occurs at the interface between the top of the sea water column and the ice bottom. However, the interaction between the tides and the ice cover (both sea ice and grounded ice) is poorly known and still not well modelled, although the friction between the ice and the water due to the tide motions is an important source of energy dissipation and has a direct impact on the ice melting (Padman and Siegfried, 2018).

The question of the impact of the sea ice on the tides in the Arctic has been investigated by different groups (Godin, 1980 & 1986; Kowalik and Proshutinsky, 1994; St-Laurent et al., 2008; Kagan and Sofina, 2010; Müller et al., 2014; Kulikov et al., 2018; Rotermund et al., 2021). They generally observe that the seasonal variations of the global patterns of the M2 semidiurnal tide (the main tidal component in the Arctic Ocean) are minor in open ocean regions and in basins that are connected to the open ocean through deep channels. By contrast, the impact of the seasonal sea ice cover friction can reach several centimeters in terms of tidal elevations in semi-enclosed basins and on the Siberian continental shelf.

In the context of climate change in the Arctic Ocean, not only the extent of the sea ice cover shrinks decade after decade, but the average ice thickness has also significantly reduced. In present time, contrary to early climate change era, most of the ice is first-year ice, i.e. formed in the year, and multi-year ice is in permanent decline (Kwok, 2018; Comiso, 2012). Climate change not only affects the extent but also the nature and the thickness of the sea ice, and this may have an impact on Arctic tides, as young thin ice is more subject to breakage than older thicker ice, which may lead to less friction at the water-ice interface.

To investigate the impact of Arctic Ocean sea ice change on ocean

* Corresponding author.
E-mail address: Ergane.fouchet@noveltis.fr (E. Fouchet).

https://doi.org/10.1016/j.ocemod.2025.102590
Received 5 October 2023; Received in revised form 7 March 2025; Accepted 1 July 2025
Available online 2 July 2025
1463-5003/

tides, it is necessary to account for the friction occurring at the bottom of the ocean ice shelves and sea ice (ice/free ocean water interface) in addition to the ocean bottom friction. However, the precise parameterization of the sea ice cover friction at the top of the water column is very complex. Indeed, the friction coefficient depends upon the micro to macro morphology of the ice base, which itself can vary with the age of the ice and/or the conditions where it was formed and further transported and modified. Also, the friction drag is a function of the velocity difference between the ocean upper layer and the ice displacement, which knowledge would require a full sea-ice modelling module in the hydrodynamic model. Implementing such a module would be at the price of a considerable increase of the modelling system complexity, with no guaranty of getting a proper answer today.

To overcome these difficulties, a very common strategy consists in implementing an empirical approach, such as defining polygons for different areas covered by sea ice, each of them being assigned an empirical value of sea ice friction coefficient. These values can be tuned in a trial/check process based on comparisons with validation observations (such as tidal elevation), retrieved by using optimal control technics, or relaxed in data assimilation approach. In the case of sea ice, the coverage of ice will strongly depend on the seasons, and the model friction will need to be modulated accordingly.

The most basic solution consists in considering that, in regions covered with sea ice, the friction parameter is a combination of the friction at the bottom and at the top of the water column. The simplest approach is to multiply the friction by a given factor (for example by a factor of two, such as in Lyard, 1997) in the regions covered with sea ice. A more complex approach consists in considering that, in this combination between the friction at the bottom and the friction at the top of the water column, the friction due to the sea ice depends on the sea ice concentration (Dunphy et al., 2005; Hannah et al., 2008; Collins et al., 2011; Kleptsova and Pietrzak, 2018).

Among many other applications, tidal models are used to remove the barotropic tidal signals from satellite altimetry observations and retrieve accurate sea surface height estimates. Today, the sea ice cover is not considered in any of the reference tidal models (ice-free solutions) used in the operational altimetry products distributed by the space agencies (e.g. GOT4.10 (Ray, 2013), FES2014 (Lyard et al., 2021), FES2022 (Carrère et al., 2022)). Hence, exploring the sensitivity of such a model, not only to the presence of sea ice but also to the evolution of the sea ice cover over time, is of prime importance to start quantifying the uncertainties in the current tidal estimates used to correct satellite altimetry observations in polar regions.

In this paper, we investigate the response of a hydrodynamic tidal model to the friction under the sea ice cover, in order to better understand the linkages, and generate more realistic simulations in the future. Specific developments have been implemented into the model to take into account the specificities of the sea ice cover and parameterize its friction with the top of the water column. We then considered different time scales, from seasonal to inter-annual, to analyze the impact of the sea-ice cover on the ocean tide simulations, both at the Arctic Ocean scale and at global scale.

This work is part of the ARKTALAS Hoavva study funded by the European Space Agency under the Contract 4000127401/19/NL/LF.

2. Data and methods

2.1. Hydrodynamic simulations

For the tidal simulations, we used the TUGO-m hydrodynamic model, which is developed at LEGOS. TUGO is a 2-D/3-D unstructured grid model based on the Navier–Stokes equation in the Boussinesq approximation. It can be used either in time domain, i.e. running a long enough time-stepping simulation (e.g. one year) and then performing tidal harmonic analyses on the resulting tidal elevations and velocities, or in the frequency domain, i.e. directly solving the tidal wave equations for each tidal component separately (starting with the velocity dominant wave to quasi-linearize friction terms). Both time and frequency domain 2D solvers are derived from the semi-implicit, shallow-water wave equation formulation, projected on Lagrange P1 basis functions for the time stepping approach, and on Lagrange P2 for elevations and discontinuous P1 for velocities for the frequency domain approach. Details on model 2D equations can be found in Lyard et al., 2006 for the frequency domain solver, and in Lynch and Gray, 1979, for the time stepping solver. The frequency domain approach is dramatically more efficient in terms of computation time, and provides equivalent results compared to the time-stepping mode for the main linear tidal components. We used the frequency domain approach for all the simulations performed in this study. The model forcing terms are the astronomic potential and tidal open boundary conditions (OBCs), plus the loading and self-attraction (LSA) terms (OBCs and LSA being extracted from FES2014 atlases). In most applications, the main tuning parameters are bottom / ice-shelf friction and internal tide drag coefficients. However, internal tide drag is of limited amplitude in polar seas, and ice shelves are of very limited extent in the Arctic Ocean, so most of the configuration calibration is performed through friction adjustment.

The bottom drag is formulated as follows in the model, starting from the vertical, standard log-profile assumption (Eq. (1)), where z is the distance to wall (ocean bottom or sea-ice), z_0 the frictional roughness, and u* the frictional velocity.

$$\boldsymbol{u}(z) = \frac{\boldsymbol{u}^*}{\kappa} \ln\left(\frac{z}{z_0}\right) \tag{1}$$

The depth-averaged velocity can be expressed as (Eq. (2)), where H is the water column thickness.

$$\bar{\boldsymbol{u}} = \frac{\boldsymbol{u}^*}{\kappa}\left(\frac{H}{H-z_0}\left(\ln\left(\frac{H}{z_0}\right)-1\right)+\frac{z_0}{H-z_0}\right) \tag{2}$$

With τ the frictional drag (not depth-averaged) and ρ the water density: $\tau = -\rho \boldsymbol{u}^{*2} = -\rho C d \bar{\boldsymbol{u}}^2 = \rho \frac{\boldsymbol{u}^*}{\kappa} \ln\left(\frac{z}{z_0}\right)$

The equivalent dimensionless bottom-drag Cd yields (Eq. (3)), which is the formulation used in the model for this study.

$$Cd = \kappa^2\left(\frac{H}{H-z_0}\left(\ln\left(\frac{H}{z_0}\right)-1\right)+\frac{z_0}{H-z_0}\right)^{-2} \tag{3}$$

As the frictional roughness is usually much smaller than water column thickness H, the friction coefficient tends to the asymptotic value of (Eq. (4)).

$$Cd \approx \kappa^2\left(\ln\left(\frac{H}{z_0}\right)-1\right)^{-2} \tag{4}$$

New developments have been implemented in the TUGO-m model to allow more flexibility in the way to handle the friction with the ice, in particular for the sea ice. The legacy, and quite limited, T-UGOm method to take into account the ice frictional effects, is to double the bottom friction coefficient (thus assuming similar roughness at the ocean bottom and below the floating ice) inside regions defined by polygons given as input parameters to the hydrodynamic model. This is an obstacle to investigate optimal ice bottom roughness value, to include the numerous smaller floating ice shelves (mostly found in the Antarctic regions) in the model input polygons, and to represent varying sea ice cover effects. New input settings for ice frictional effects have thus been implemented in T-UGOm, both to provide a more flexible ice roughness setting, and to allow for more precise and possible time varying ice cover. In the end, the total friction considered in the model is the sum of the bottom friction and the ice friction.

A run-time level, ice thickness raster-based method has been implemented to define the ocean ice shelves cover. Ice-shelf thickness raster inputs such as the RTopo-2.0.4 global dataset (Schaffer et al., 2019) can now be directly used by the model. A similar sea ice concentration raster-based method has been implemented to define the sea ice cover and tested from the NSIDC daily and monthly products (https://nsidc.org). A pre-processing step is necessary to handle the NSIDC products and to aggregate the daily or monthly files into a unique annual input file containing the corresponding time frames. Last but not least, the ice friction parameters setting has been dissociated from the ocean bottom one. It allows for choosing between the different parameterization used in friction computation (Nikuradse law, Manning or Cd coefficients), and for prescribing specific friction parameters values in regions defined with polygons. In particular, it allows for specifying different frictions for ice shelves and sea ice, and potentially to locally modulate sea ice friction to account for roughness heterogeneity due to actual local ice age or state (compact, fractured …).

The sea ice roughness's setting in numerical models still remains mostly simple, arbitrary and at the best empirical. Not only the basic knowledge about the sea ice bottom roughness itself is barely known, but this is the case also for the sea ice motion, necessary to compute the differential velocity with the ocean surface level needed by the friction stress derivation. In the tidal simulations presented in this paper, we have used a uniform roughness length for the whole domain. The treatment of ice motion effect is also quite basic. Below an arbitrary sea ice concentration threshold (typically 0.7 for concentration ranging between zero and one), sea ice is considered to freely follow tidal flow, hence triggering no or negligible friction effects. The sea-ice friction coefficient then linearly increases from the concentration threshold up to the maximum concentration, for which sea ice can be considered as land-fast, at least at tidal period time scales.

However, using a uniform sea-ice concentration threshold value does not account for the ocean geometry constraints on sea ice displacement. Depending on the threshold value, it tends to over-estimate the sea-ice friction effects in the open sea and/or underestimate them in narrow channels or close to the shoreline. To overcome this issue, a confinement length representing the ocean geometry constraints has been defined by computing a characteristic "free water extent" length, based on an ad hoc transform of minimum distance to coast metrics. The confinement allows for tuning the threshold value (typically 0.7 in confined areas up to 0.9 in open sea areas). Comparisons to tide gauges for the two approaches (with and without confinement) provide very close results, with submillimetric differences. From this we can conclude that the confinement approach does not degrade the simulations in regions where we have observations. However, most of the tide gauge stations selected for this study (covering the whole simulation period discussed hereinafter) are unfortunately not located in the regions where the impact of the confinement approach is the largest (see Fig. 1 for the regions where the confinement approach has an impact and Fig. 2 for the tide gauge stations). The range of vector differences between summer and winter M2 tidal simulations with and without the confinement approach (Fig. 1) can be considered as well above model uncertainties in many places, although quantifying those uncertainties is a difficult matter considering the sparsity of in situ or satellite altimetry observations in the polar seas and the tidal non-stationarity due to sea ice variability. On average, the accuracy of T-UGOm based simulated tidal constituents is of the order of 1.5 cm or less in the deep ocean, and 5 cm or less in coastal areas, after model configuration calibration. More detailed estimates can be either found in the former publication about Arctic Ocean tides (Cancet et al., 2018) or in FES atlases publications (where non-assimilated solutions are discussed). The largest impact of the confinement approach can be observed along the coasts of the western Hudson Bay, and in the Hudson Strait, between the Baffin Sea and the Hudson Bay (Fig. 1). This region is of particular importance as there is tight connexion between the Hudson Bay and the whole Atlantic Ocean in terms of tidal energy fluxes. The maximum winter-summer differences we obtain on M2 from tide gauge observations are observed at the Churchill tide gauge station in the western part of the Hudson Bay, where they reach 10 cm in the 1980s to 1990s period, while the model gives >20 cm of vector difference without the confinement approach and about 15 cm with the confinement approach (see Section 3.3 and Appendix for all comparisons between the model and the tide gauges). However, the evolution over time of the seasonal variations of tides at the Churchill tide gauge is questionable (see Section 3.3) and makes it difficult to use as a sound reference for model validation. In the Hudson Strait, the confinement approach reduces the vector differences on M2 between summer and winter simulations, from >20 cm without confinement to 10 to 14 cm locally with confinement, considering that the sea ice can move within the 400 km wide strait and thus leading to less tidal energy dissipation in the presence of sea ice. Here again it is

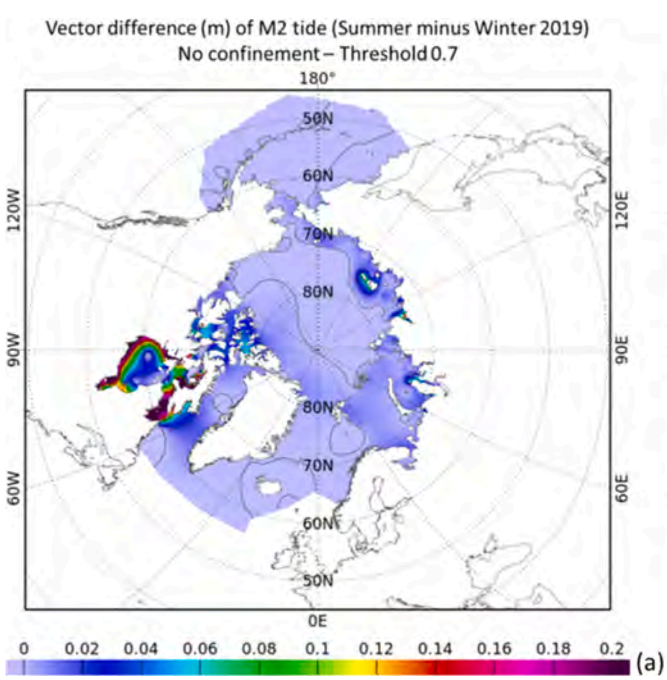

Fig. 1. Impact of confinement modulation of sea ice friction by the confinement length parameterization, winter/summer differences in M2 tide (vector difference in meters) for 2019, without confinement modulation (a), with confinement modulation (b).

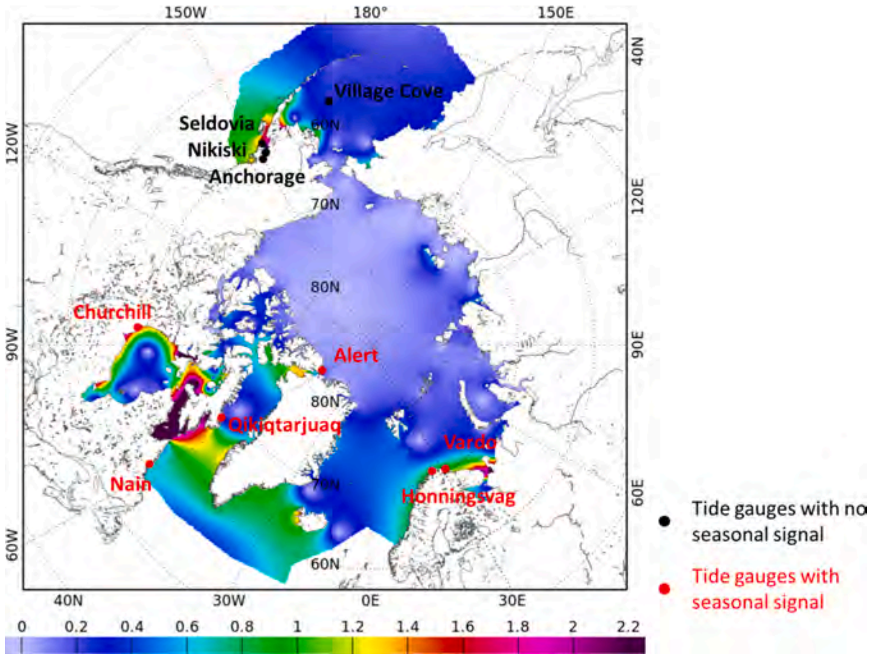

Fig. 2. Amplitude (in m) of the M2 tidal component from the regional model considering no sea ice cover, and locations of the tide gauge stations considered in the study.

difficult to evaluate the real accuracy of this result as there is no long-enough time series of in situ observations in this area that we could compare with our simulations. Unfortunately, we could not find in situ estimates of the seasonal tidal amplitude variations in this region in the literature, and other studies in the area report differences of 20 cm to 50 cm between observations and model simulations (St-Laurent et al., 2008; Kleptsova and Pietrzak, 2018), which correspond to several orders of magnitude of the seasonal variations we observe. We thus propose this approach as a first step to handle sea ice in our model, knowing that further analyses and developments are certainly required to obtain more realistic simulations but made difficult by the lack of exploitable validation data.

For the regional simulations over the Arctic Ocean, we used the Arctide2017 regional model configuration described in Cancet et al., 2018, with a number of improvements. First, the Hudson Bay and the Foxe Basin were added to the model domain, which strongly improves the model tidal estimates in the Baffin Bay. Second, the model domain was extended South of Iceland and South of the Bering Strait, in order to reduce model instabilities due to the interactions between the tides and locally steep bathymetry gradients that had been identified in the Arctide2017 configuration. Finally, recent bathymetry datasets have been assessed and merged into the model bathymetry where relevant (BedMachine Arctic (Morlighem et al. 2017), GEBCO-2020 (https://www.gebco.net), and NOAA data in the Anchorage Bay). The standard configuration of this regional model, i.e. without considering any sea ice cover, has been calibrated and validated against satellite altimetry and tide gauges observations (see Sections 2.2 and 2.3).

The global configuration used for this study is the FES2014 one, described in Lyard et al., 2021. Except for the sea ice cover aspect, the only other addition to the FES2014 hydrodynamic configuration is the use of the RTopo-2.0.4 ice-thickness map to define the ice-shelf regions in Antarctica, whereas only very basic polygons were used in the FES2014 original configuration, over the Amery ice shelf and the ice shelves in the Weddell Sea and in the Ross Sea. The validation of the FES2014 hydrodynamic simulation is described in details in Lyard et al., 2021.

Cancet et al. (2018) present an assessment of both the Arctide2017 regional and FES2014 global hydrodynamic simulations in the Arctic Ocean, and demonstrate the improvement brought by the regional configuration in the area, thanks to higher resolution combined with more accurate bathymetry information, and regional tuning of the model parameters. In this study, we take advantage of the higher performance of the regional configuration to explore in details the impact of changing sea ice cover at some local stations that are not so well resolved in the global model. The global simulations are used to investigate the long-distance influence of the interactions between the Arctic sea ice cover and the ocean tides.

To evaluate the impact of the evolution of the sea ice cover on the ocean tides in the Arctic Ocean and at global scale, a series of simulations was performed in the frequency domain (i.e. directly solving the tidal wave equations) for the M2 and K1 main tidal components, for a time period ranging from 1980 to 2020 and considering seasonal sea ice concentrations to simulate the seasonal variations of the tides due to the sea ice cover. The seasonal sea ice concentration maps were computed using the NSIDC monthly sea ice concentration products provided in GEOTIFF format, available from 1979 to today. For the global simulations, global maps of the Arctic and Antarctic sea ice concentration were built from the NSIDC products to feed the hydrodynamic model with a single map for each simulation. For each year, the seasonal maps were computed as the mean of the monthly sea ice concentration maps over three months: Winter (January, February, March), Spring (April, May, June), Summer (July, August, September) and Fall (October, November, December). The range of sea ice concentration considered by the model was set to 0.7–1.0 (i.e. 70 % to 100 %) in order to limit the introduction of additional friction because of possible artefacts in the low sea ice concentration estimates.

For both configurations (regional and global), we performed one hydrodynamic simulation for each season of each year from 1980 to 2020 (i.e. 164 simulations of M2 and K1 for each configuration).

2.2. Satellite altimetry observations

Satellite altimetry sea surface height measurements sample the global ocean tide signals at each revisit of the satellite. Because the satellite revisit period is of several days, the high frequency tidal signals are projected onto much longer aliasing periods, as presented in Table 1.

Table 1
Aliasing periods of the main tidal components depending on the satellite repeat cycle.

Tidal component	Topex/Jason 9.915600-day orbit Latitude max. 66°	Sentinel-3 27-day orbit Latitude max. 82°	ENVISAT/SARAL 35-day orbit Latitude max. 82°	CryoSat-2 368.2396-day orbit Latitude max. 88°
M2	62 days	157 days	94 days	800 days
S2	59 days	Inf.	Inf.	768 days
K1	173 days	365 days	365 days	1486 days
O1	46 days	277 days	75 days	1262 days

In general, the Topex/Jason repeat orbit of about 10 days is the most favourable to estimate the tidal harmonic constituents (amplitude and phase lag) from satellite altimetry time series. In the case of sun-synchronous orbits such as ENVISAT, SARAL and Sentinel-3, the S2 main solar tide component is aliased to an infinite period and cannot be estimated. For all the missions, time series of several years of observations are necessary to accurately separate the various tidal components thanks to harmonic analysis processing. In the Arctic Ocean, the spatial coverage of the Topex/Jason suite missions is limited to 66°N. In addition, the conventional altimeters are strongly impacted by the intermittent presence of sea ice (Armitage et al., 2016; Prandi et al., 2012), which leads to seasonal gaps in the time series and degrades the tidal estimates. Unfortunately, the satellite altimetry missions that reach higher latitudes and provide the longest time series in the Arctic Ocean (ERS-1/ERS-2/ENVISAT/SARAL) are sun-synchronous, which affects the tidal retrievals and the possibility to accurately separate some of the tidal components (like K1 and P1, for which the separation period is infinite is such cases). Sentinel-3A&B are also on sun-synchronous orbits, spatially shifted from the ENVISAT orbit. With >10 years of measurements up to 88°N on a non-sun-synchronous orbit, the CryoSat-2 mission provides invaluable sea surface height observations that can be analysed to accurately estimate the tidal harmonic constituents, despite its long-period repeat cycle. In addition, the SAR and SARin modes of the altimeter are less affected by the presence of sea ice, thanks to their higher along-track resolution.

We have estimated the tidal harmonic constituents from the CryoSat-2 sea surface height measurements, considering >11 years (July 2010 to December 2020) of observations. We used the ESA Level-2 GOP Baseline C products, which provide sea surface height information for the three modes of the altimeter (LRM, SAR and SARin) and thus cover the whole Arctic Ocean, up to the orbit limit of 88°N. In order to improve the separation of the tidal components, the altimetry observations were binned into cells of 1° by 1° and time series were built in each cell. A prior tidal solution, based on the regional Arctic model configuration, was removed from the altimeter sea surface height before performing harmonic analysis, and then restored into the computed tidal constituents.

Because time series of >10 years are needed to accurately estimate the tidal harmonic constituents from the altimetry observations, the CryoSat-2 tidal estimates are representative of average tides over the most recent period (2010–2020). They were thus used to tune the model parameters and for comparison purposes with the model simulation in the generic configuration, without considering any sea ice cover. The ENVISAT observations could be used to estimate the tidal constituents for the period 2002–2012, but the signal to noise ratio is less favourable as explained above, and the uncertainties in the tidal estimates can reach several centimetres. Finally, because the satellite altimeter radar signal is affected by the presence of sea ice, the computation of seasonal tidal estimates from satellite altimetry observations, separating Summer and Winter data for example, results in uncertainties of several centimetres in sea-ice covered regions, i.e. in the range of the seasonal differences that can be observed in the tidal estimates at tide gauges. For this reason, we did not use such approach for this study. However, the publication of a new polar altimetry tidal dataset (Andersen et al., 2023) based on reprocessed CryoSat-2 data may be of interest for such considerations in the future (not available at the time of the present study).

2.3. *Tide gauge in situ observations*

In order to compare the model results with independent observations at seasonal time scale, and on a longer period than the recent satellite altimetry era, we considered long time series of hourly tide gauge measurements. We used data from the GESLAv3 database (Haigh et al., 2021), completed with more recent data from the UHSLC database (Caldwell et al., 2015) where available and relevant. Although a large number of tide gauge stations can be identified in the Arctic Ocean, most of the time series are very short (a few weeks to a few months) and often prior to 1980. In particular, most of the Canadian tide gauge observations in the Canadian Archipelago and in the Hudson Bay were collected in the 1970s. Based on the statistical analyses performed on the seasonal tidal simulations (see Section 3), we have identified eight tide gauge stations (see Fig. 2) located in regions of interest in terms of tidal amplitude, and that more or less cover the 1980–2020 period, in general with gaps of several months (up to several years), especially in the 1980–1990s period: the Honningsvag and Vardø stations are located on the northernmost coast of Norway, the Fort Churchill station is located in the Hudson Bay, the Alert station is located in the northern part of the Canadian Archipelago, close to Greenland, the Anchorage, Nikiski and Seldovia stations are located in the Anchorage Bay, and the Village Cove station is located in the Bering Strait. In addition, two stations located in the Baffin Bay (Nain and Qikiqtarjuaq) were considered although they provide much shorter time series, starting only in 2006 with many gaps.

Each hourly time series was carefully verified, and split into three-month subsets corresponding to the seasons previously defined. Harmonic analysis processing was then performed on each seasonal subset, in order to obtain time series of seasonal tidal constituents (amplitude and phase lag) for the main tidal components (M2, K1, S2 and O1 mainly). The stations were separated into two subsets, corresponding to those that highlight a clear seasonal tidal signal (in red on Fig. 2) and those with no seasonal tidal signal (in black).

3. Results

3.1. *Sea-ice related variability in tidal elevations*

The seasonal changes in sea ice cover modulate the associated ocean/sea ice friction over the year. The effect on tide can be significant if changes occur in regions where the tidal currents are large, with local and possibly remote effects. In addition, and because of the effect of climate change, the sea ice cover is diminishing decades after decades. This raises the question of the rate of change of Arctic tides due to this evolution, and possible subsequent changes in tides in other parts of the world ocean. For most science or engineering applications, the barotropic tides are usually considered as unchanging, and at some limited degree of accuracy, this is a perfectly workable assumption. However, in some more demanding tidal applications such as satellite altimetry corrections, which require the best available tidal prediction accuracy and consistency, the seasonal, inter-annual and long term changes in tidal amplitude or phase, in particular those linked with sea ice concentration variability (Fig. 3 and Fig. 4e), can become an issue.

Because of the global warming effects, the sea ice concentration is decaying in the Arctic Ocean, with a large, clearly visible diminution of the sea ice cover in the central Arctic Ocean during the "warm" season (see Fig. 3). Because of the rather weak tidal currents in this region, this has probably a minor impact on tides. Even in the absence of long term changes, the seasonal changes in sea ice are not exactly the same from one year to another, in terms of intensity and timing. Fig. 4 (a to d) shows the sea-ice cover variability for each season (standard deviation of seasonally averaged concentrations) over the 1980–2020 time period.

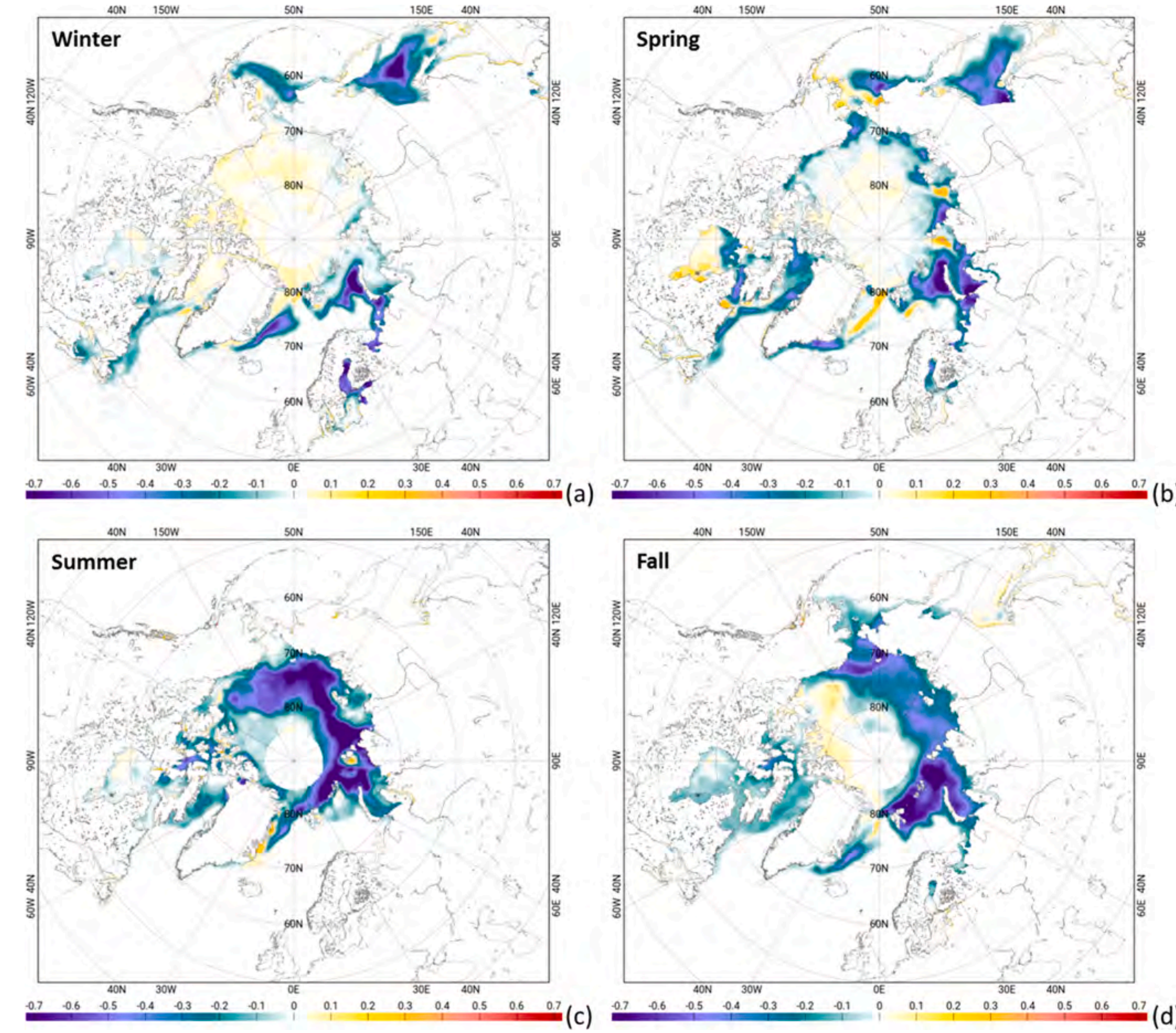

Fig. 3. Difference of seasonal sea ice concentration (NSIDC products) between the years 1980 and 2020 (2020–1980) for winter (a), spring (b), summer (c), fall (d).

The standard deviation reaches values as high as 30 % of the maximum concentration, which is a rather large proportion. Again, effects on tides are expected to be limited to regions where tidal currents are large, such as the Canadian Archipelago and the vicinity of the White Sea. The overall variability of the sea ice concentration computed from all seasons over the 1980–2020 time period (Fig. 4e) shows larger values than the variability per season because of the dominant seasonal variability.

In the following, we will assume that most of the sea-ice-induced tidal changes are dominated by seasonal and inter-annual variability, focusing on standard deviation to illustrate this variability.

3.2. Regional simulations over the 1980–2020 period

To address possible changes in Arctic tides at various scales (seasonal, inter-annual and long-term), we have produced tidal simulations with seasonal sea ice conditions processed for each year from 1980 to 2020, considering the sea-ice friction scheme depending on the seasonal sea ice concentration (default threshold of 70 %, modulated by ice confinement). In the following, only the cases of M2 and K1, the main tidal components in the region, are discussed. We recall here that our simulations are performed in the frequency domain, hence only tidal elevations and velocities are estimated (no other ocean processes) and we can thus directly link the changes in the tidal estimates with the sea ice information ingested by the model.

First, the overall tidal variability (complex standard deviation) computed over the 1980–2020 time period from all seasonal solutions (Fig. 5e for M2 and Fig. 6e for K1) shows larger values than the variability per season (Fig. 5a-d for M2 and Fig. 6a-d for K1) because of the dominant seasonal variability. The regions that show the largest overall variability are the Hudson Bay and the Canadian Archipelago, as well as the Baffin Bay in the case of K1.

For the M2 tide, the variability computed from the seasonal atlas is maximum (reaching about 3 cm locally) in winter and spring conditions (Fig. 5a and b). This is likely linked with the much reduced sea ice cover in summer/fall seasons (Fig. 5c and d) compared to winter/spring seasons, hence minimizing the sea ice climatic changes effects. During winter and spring, the Hudson Bay, the Foxe Basin and the White and Kara Seas are the regions showing the most significant modifications. The summer and fall conditions are much less affected (locally 1 to 2 cm), and mostly in the Canadian Archipelago and along the Siberian

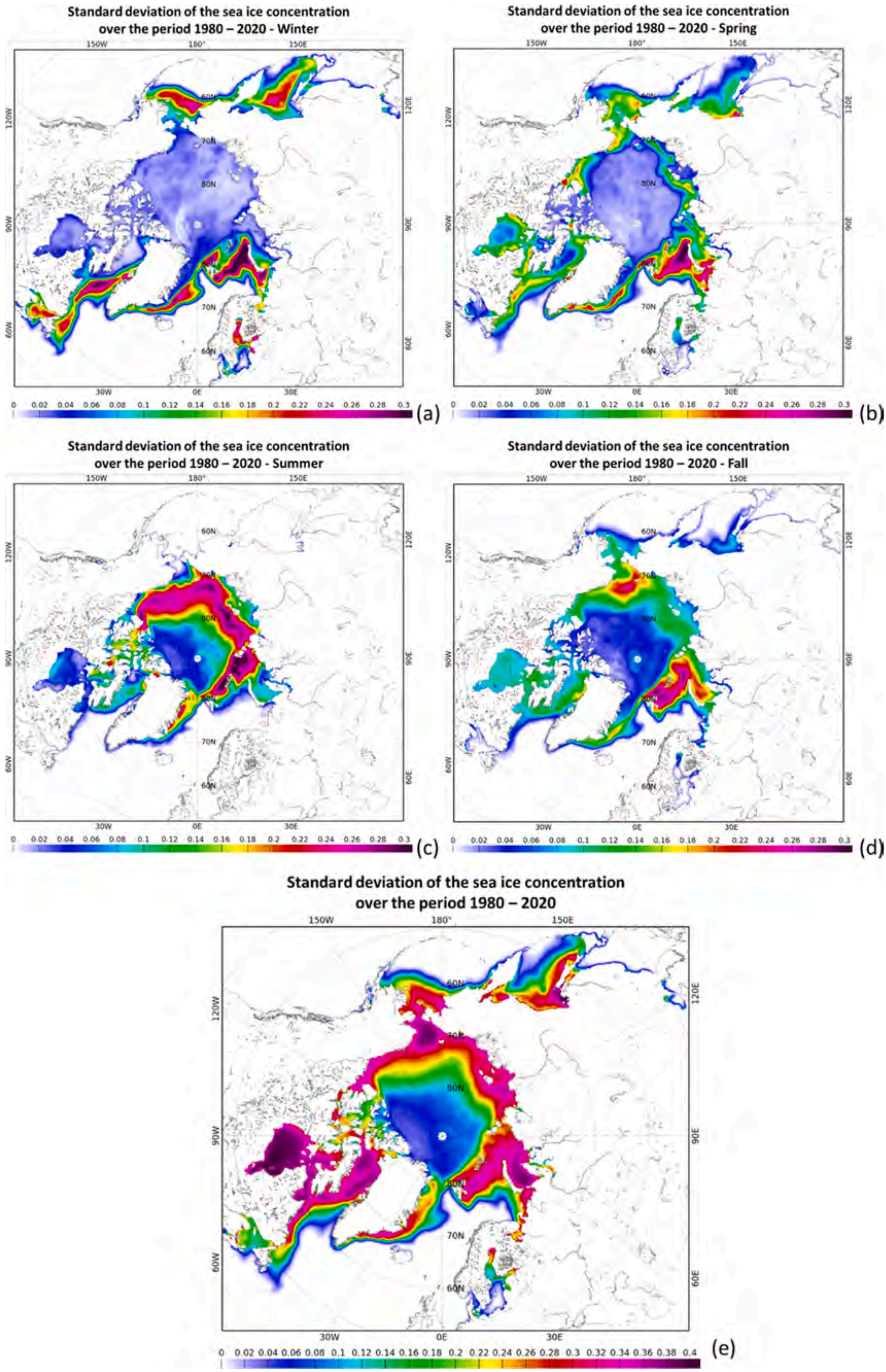

Fig. 4. Standard deviation of sea ice concentration (ranging from 0 to 1) over the 1980–2020 time period (NSIDC products): winter (a), spring (b), summer (c), fall (d), and all seasons combined (e).

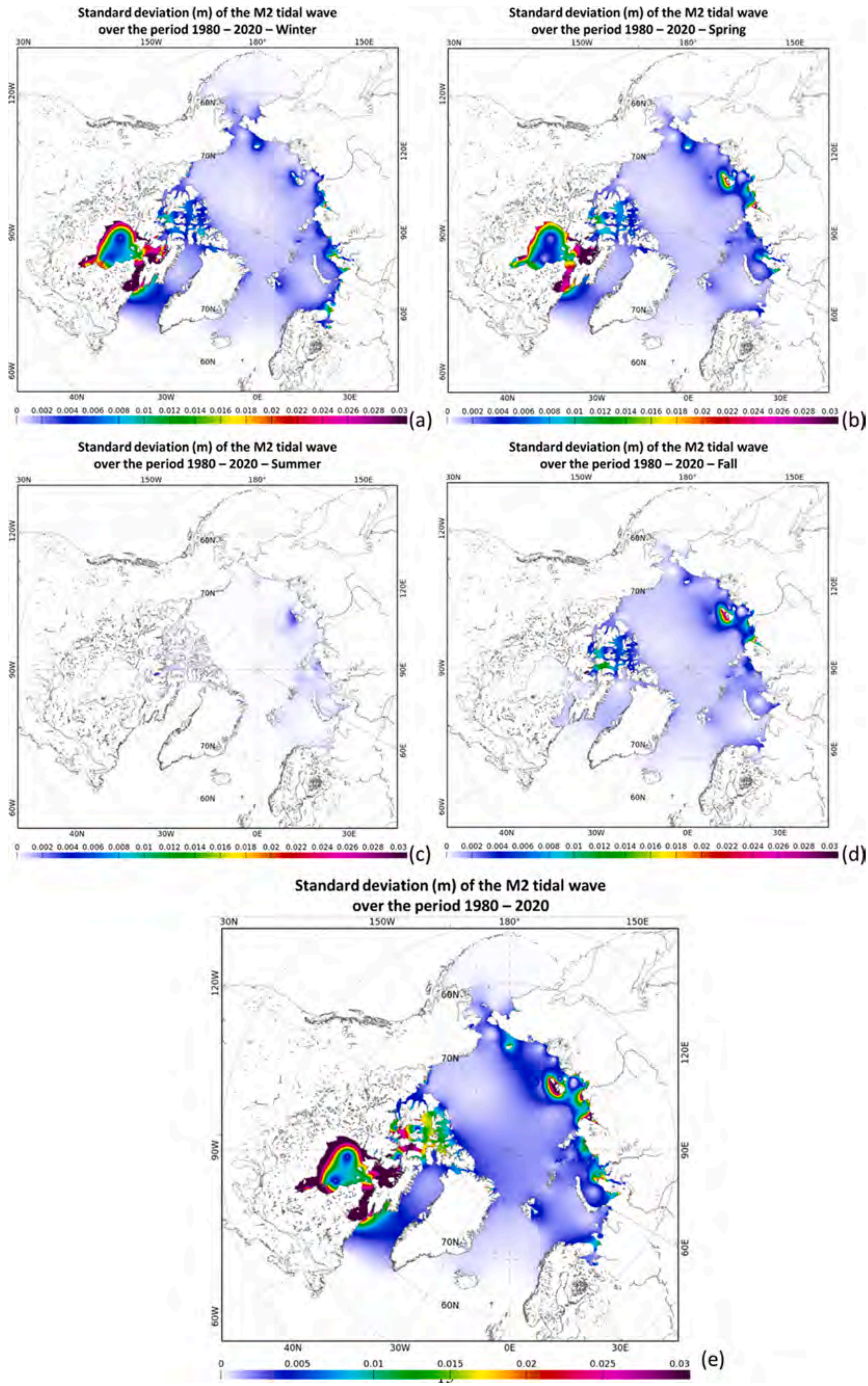

Fig. 5. Complex standard deviation (m) of the M2 tide over the 1980–2020 time period, for seasonal sea ice conditions: winter (a), spring (b), summer (c), fall (d), and all seasons combined (e).

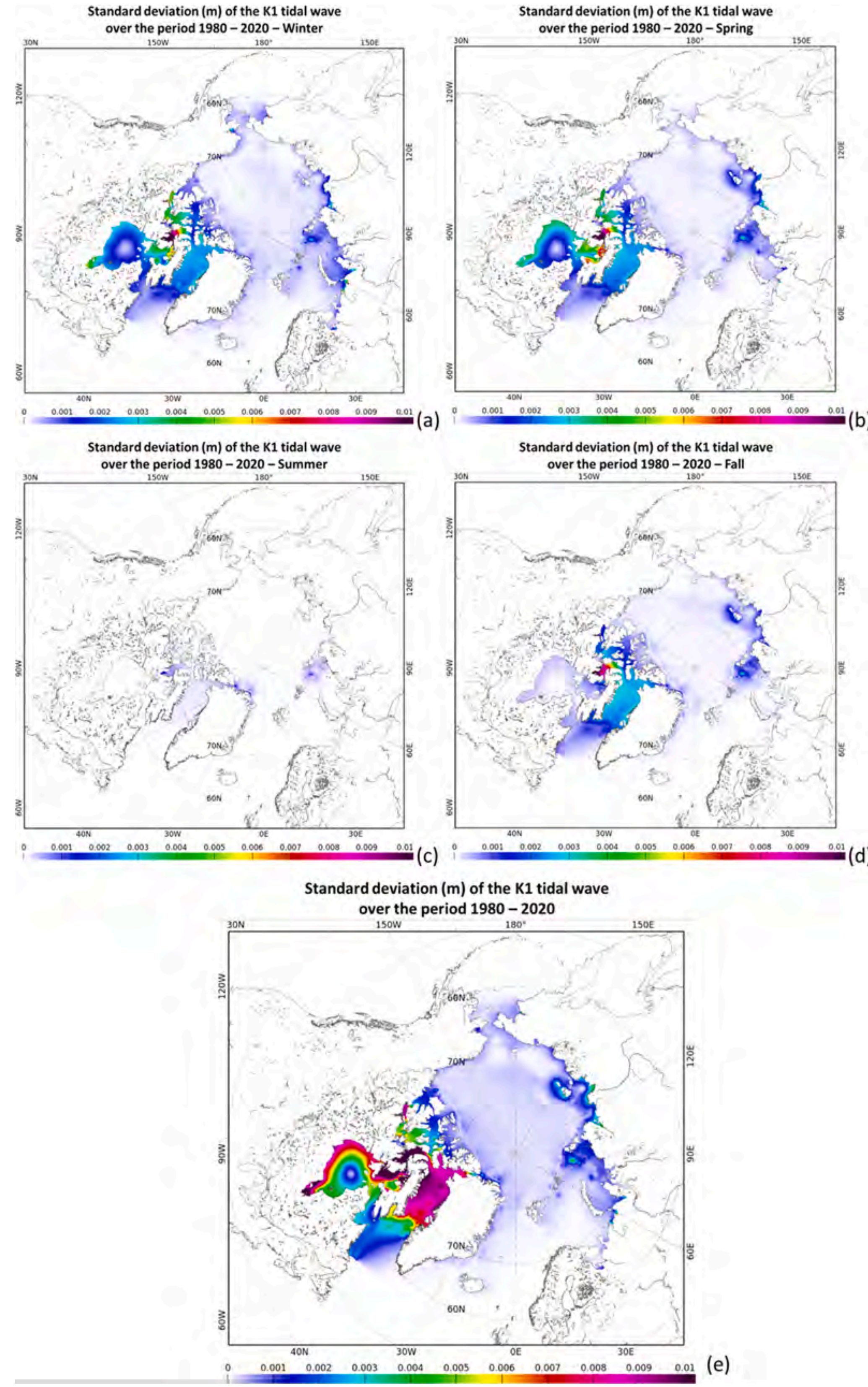

Fig. 6. Complex standard deviation (m) of the K1 tide over the 1980–2020 time period, at seasonal sea ice conditions: winter (a), spring (b), summer (c), fall (d), and all seasons combined (e).

coast.

The K1 tide case is slightly more surprising (Fig. 6). While winter and spring seasons show higher tidal changes compared to summer, the fall season displays the largest modifications, mostly in the northern Baffin Sea and in the Canadian Archipelago. The explanation can be found in the latter place, which dynamically controls the K1 resonance in the Baffin Sea and seems more affected by long-term sea ice changes in the fall season (this can also be observed for the M2 tide, without of course the diurnal resonance effects in the Baffin sea). It might explain the differences in the K1 tide that have been historically observed in this region between the various global tidal atlases (GOT, TPXO, FES). These atlases were produced at different time, and used satellite altimetry data for data assimilation or optimal mapping processing collected over epoch-dependent time periods.

3.3. Tidal variability from tide gauge data

The seasonal regional tidal simulations have been compared to the seasonal in situ tidal observations at each of the ten tide gauge stations presented in Section 2.3, for the main tidal components M2 and K1. It

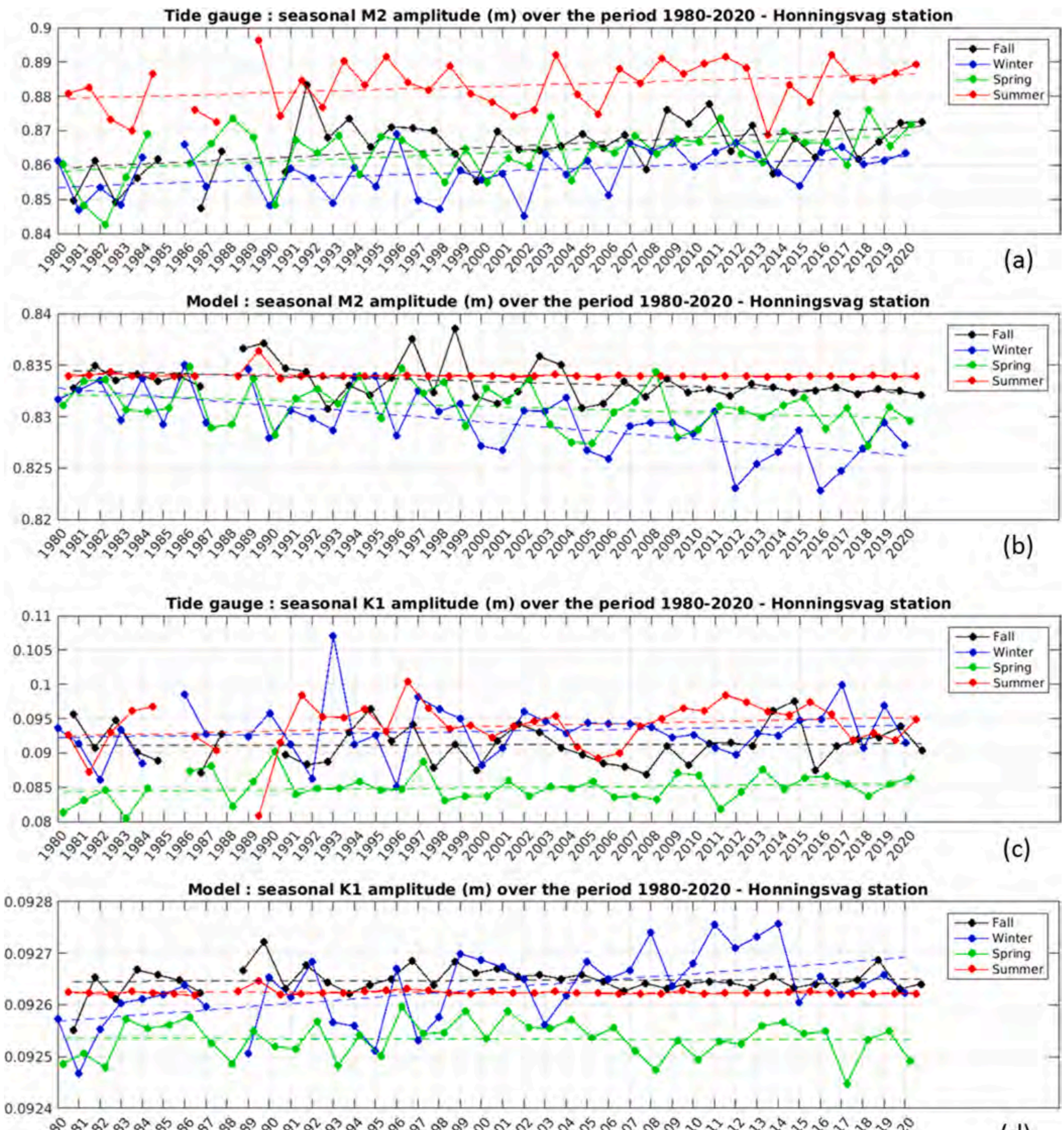

Fig. 7. Honningsvag tide gauge: seasonal tidal amplitudes for the M2 (a and b) and K1 (c and d) tides from observations (a and c) and simulations (b and d) over the 1980–2020 time period. The coloured dashed lines show the linear trends of the time series.

should be noted here that contrary to our tidal simulations, where the only changing control parameter is the sea ice cover, the variations of tidal amplitudes in the tide gauge observations can be due to many different and potentially combined reasons, including the sea ice cover changes but also possible variations in hydrography, river discharge (some stations are located in estuarine areas), water column stratification, and local bathymetry, for example. Such conditions are not considered in the model simulations.

Fig. 7 shows the seasonal times series of the amplitude of the M2 and K1 tides extracted from the model and analysed from the tide gauge data for the Honningsvåg station as an example of stations that highlight a clear seasonal cycle for tides (red dots on Fig. 2). Figures for the other stations with a clear seasonal cycle are presented in Appendix (Figure 13 to Figure 16). Fig. 8 shows the seasonal time series analysed from the tide gauge data at the Seldovia station as an example of stations with no clear seasonal cycle (black dots on Fig. 2). Figures for the other stations with no clear seasonal cycle are presented in Appendix (Figure 17 to Figure 19). We do not show the model time series for these latter stations, as they do not highlight any seasonal nor inter-annual variability (the model time series are very close to each other and completely flat).

In general, the results are very heterogeneous, depending on the in situ station, and on the tidal constituent. The set of convenient in situ data available to examine the tidal variability is extremely reduced, and the necessity to seasonally split the harmonic analysis is a source for harmonic constant analysis errors, which undermines the possibility to draw firm conclusions. In particular, 3 months of hourly tide gauge data may not be enough to accurately separate the K1 and S1 tides in the harmonic analysis process. In some stations, we can observe some qualitative agreement between simulations and observations, and significant differences can be noticed at other stations. For the M2 tide, consistently with the idea that sea ice friction will drive the tidal amplitude, the summer season amplitude is usually larger, and the winter or spring amplitudes are the weakest, but it can also be quite the opposite as can be observed at the Alert and Nain stations (see figures in Appendix).

The best agreement occurs at the two stations located north of Norway (Honningsvåg and Vardø), in a year-round sea-ice free region, where the evolution in the tidal amplitudes is not due to local effects of the sea ice cover, but may be linked with remote effects. There is a clear seasonal difference in the in situ observations at these two stations, with M2 amplitudes about 2-cm larger in summer than for the other seasons. The model also displays seasonal variations, but with lower magnitude (e.g. a few millimetres). One can also note slightly positive trends in the tidal estimates from observations for all the seasons at these in situ stations, while the model provides negative trends. Again, it should be noted here that this different long-term behaviours for the tide gauges and the model may be attributable to other hydrographic changes than the sea ice cover that are not considered in the model.

In Churchill (Fig. 9), the time series show a large decay in the M2 tidal amplitudes for all the seasons. This was already identified and investigated by Ray (2016), and no clear explanation for such an unexpected behaviour is available yet. The tide gauge is located in an estuarine region, and may be affected by some specific river regime. The CryoSat-2 altimetry observations in the area (representative of an averaged 2010–2020 period) provide M2 amplitudes of 1.4 m, but are not located exactly in the estuary like the tide gauge instrument. A slight decay is also observed for the K1 component but not at the same level, as the amplitudes are much lower (Fig. 9b). The largest changes in the seasonal sea-ice concentration at Churchill occur in spring, with a reduction over the years, and increased inter-annual variability in the sea-ice concentration since 1985. The case of the Churchill station is a typical issue and limitation to the study of long-term variations of the ocean tides in the Arctic region, as this is the only tide gauge that has provided measurements in the Hudson Bay over the whole period since the 1980s. Although about fifty stations are available in the area, the data were generally acquired in the 1970s or in the 1990s, and all the time series are too short to estimate seasonal tides (time series of a few weeks, in general in summer). Modelling is thus the most complete approach to investigate high-frequency processes such as tides in the Arctic Ocean, providing estimates over the whole ocean, and the whole

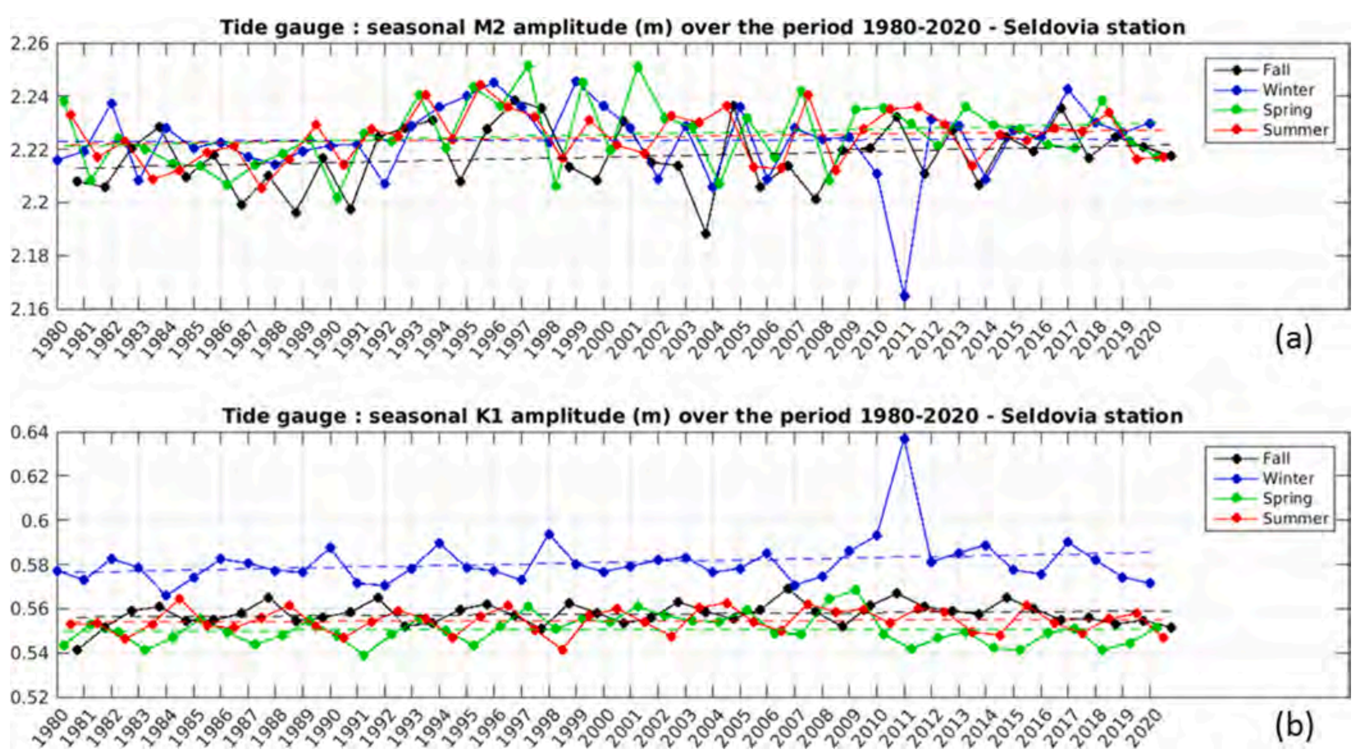

Fig. 8. Seldovia tide gauge: seasonal tidal amplitudes for the M2 (a) and K1 (b) tides from observations over the 1980–2020 time period. The coloured dashed lines show the linear trends of the time series.

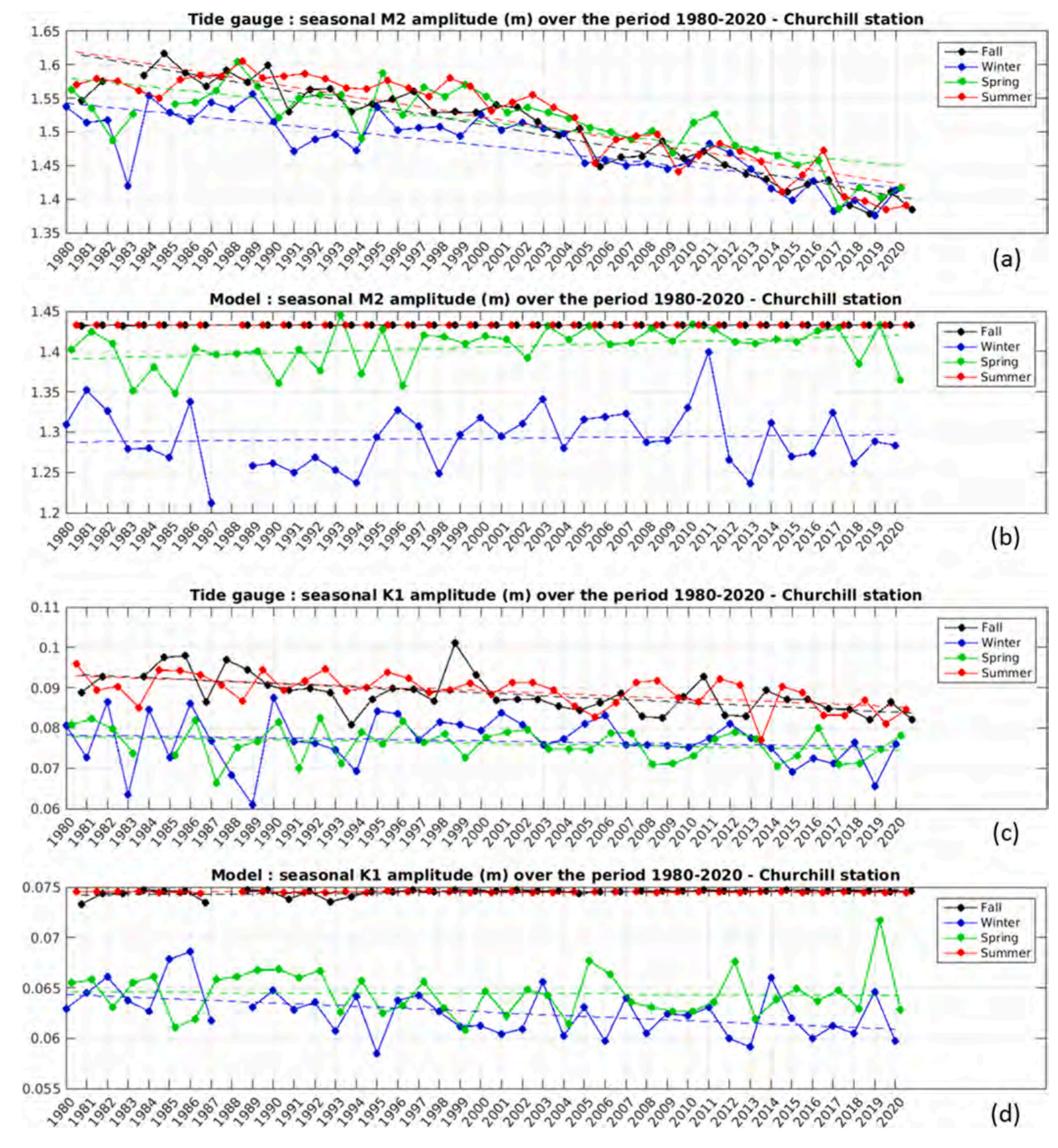

Fig. 9. Churchill tide gauge: seasonal tidal amplitudes for the M2 (a and b) and K1 (c and d) tides from observations (a and c) and simulations (b and d) over the 1980–2020 time period. The coloured dashed lines show the linear trends of the time series.

period of interest. However, there is a dramatic lack of observations to validate the model simulations, particularly in such a quickly-changing environment.

Finally, the lack of seasonal and inter-annual variability in the model simulations at the stations located in Alaska (Nikiski, Seldovia, Anchorage, and Village Cove) may reflect some lack of connection between the Pacific Ocean and the Arctic Ocean through the Bering Strait. The open boundary conditions of the model in the Pacific Ocean, constrained with the same FES2014 global solution (no seasonal or inter-annual variations) for all the seasonal simulations and for each year of the 1980–2020 period, may be located too close to the Bering Strait, and may prevent the regional model from developing its own tidal variability in the region.

3.4. Global simulations over the 1980–2020 period

In order to investigate the possible long-distance effect of the variations of sea ice cover in the Arctic Ocean, global simulations based on the FES2014 global model configuration have been performed every year over the period 1980–2020, considering the sea-ice friction scheme depending on the seasonal sea ice concentration (default threshold of 70 %, modulated by ice confinement). The only input parameter that changes from one simulation to the other is the sea ice concentration in the Arctic and Antarctic Oceans, there is no other temporal aspect in the model (runs performed in the frequency domain). For each season, the standard deviations of the M2 and K1 tidal components have been computed over the 40 years, and are shown on the maps presented on Fig. 10 and Fig. 11.

It is computed from the following formula:

$$\sigma = \sqrt{\frac{1}{2N}\Sigma_k |z_k - \overline{z}|^2} \text{ where } z_k = A_k e^{i\varphi_k}$$

A_k and φ_k are respectively the amplitude and phase of the tidal constituent, k refers to the 1980 to 2020 years considered and $N = 40$ years.

First, the overall tidal variability (Fig. 10e for M2 and Fig. 11e for K1), which is computed over the 1980–2020 time period from all seasonal solutions, shows larger values than the inter-annual variability per season (Fig. 10a-d for M2 and Fig. 11a-d for K1) because of the dominant seasonal variability. For M2, the overall tidal variability is dominant in the Arctic and North Atlantic Ocean, the Okhotsk Sea, the Arabian Sea and in the Mozambique Channel, reaching centimetre values and larger, with maximum values mostly reached in the Hudson Bay and Foxe Basin.

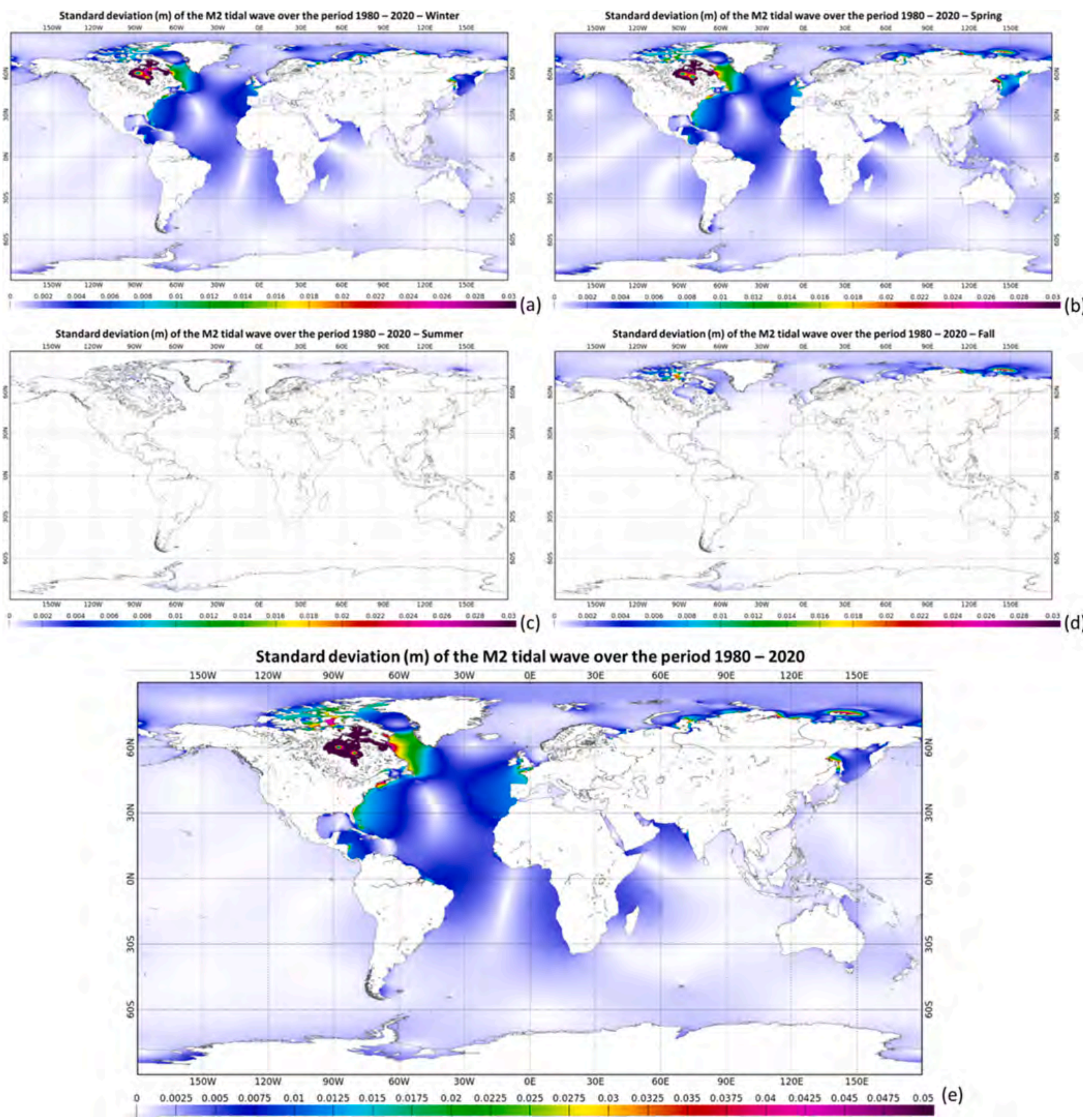

Fig. 10. Complex standard deviation (m) of the M2 tide over the 1980–2020 time period at global scale, at seasonal sea ice conditions: winter (a), spring (b), summer (c), fall (d), and all seasons combined (e).

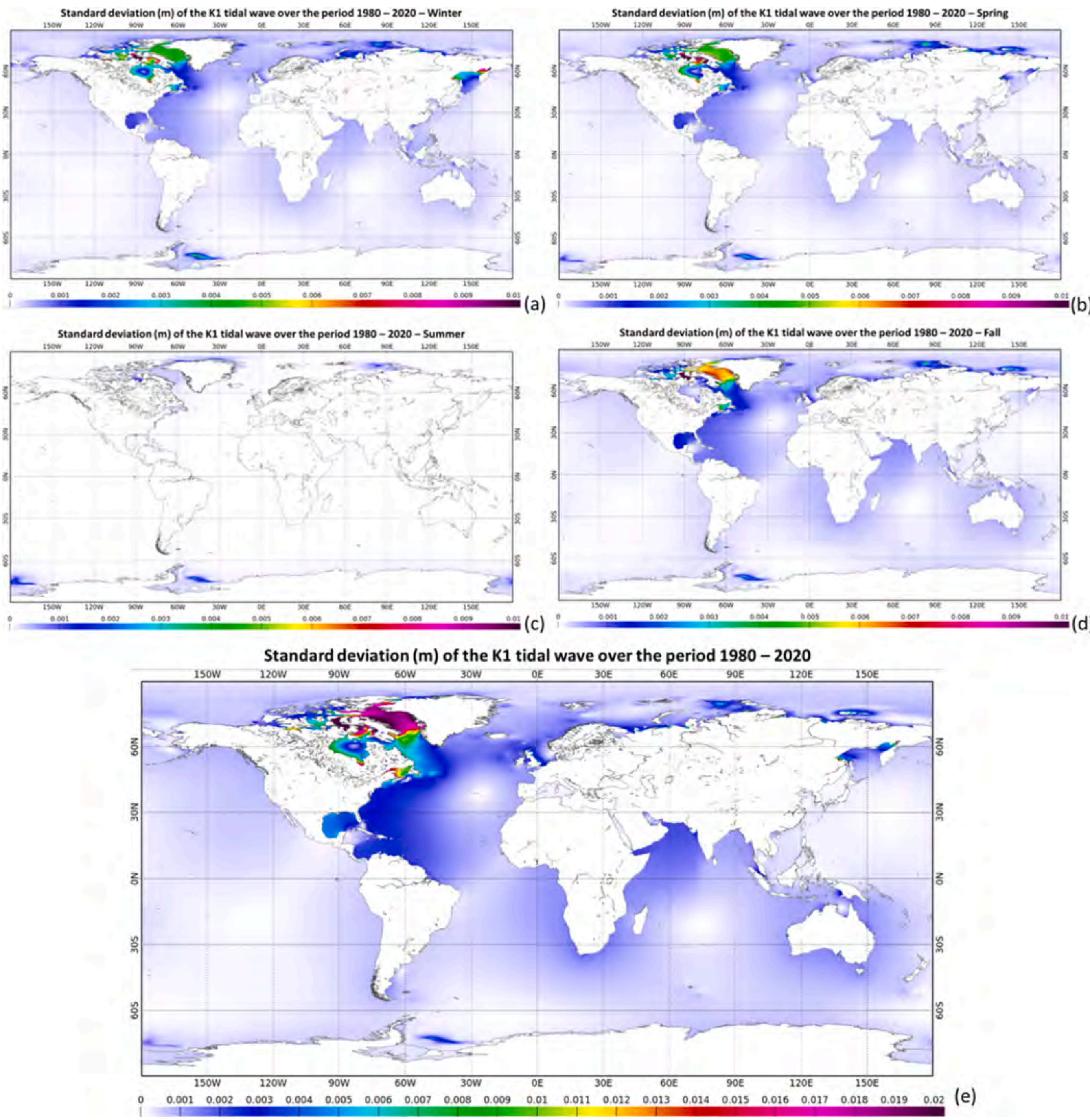

Fig. 11. Complex standard deviation (m) of the K1 tide over the 1980–2020 time period at global scale, at seasonal sea ice conditions: winter (a), spring (b), summer (c), fall (d), and all seasons combined (e).

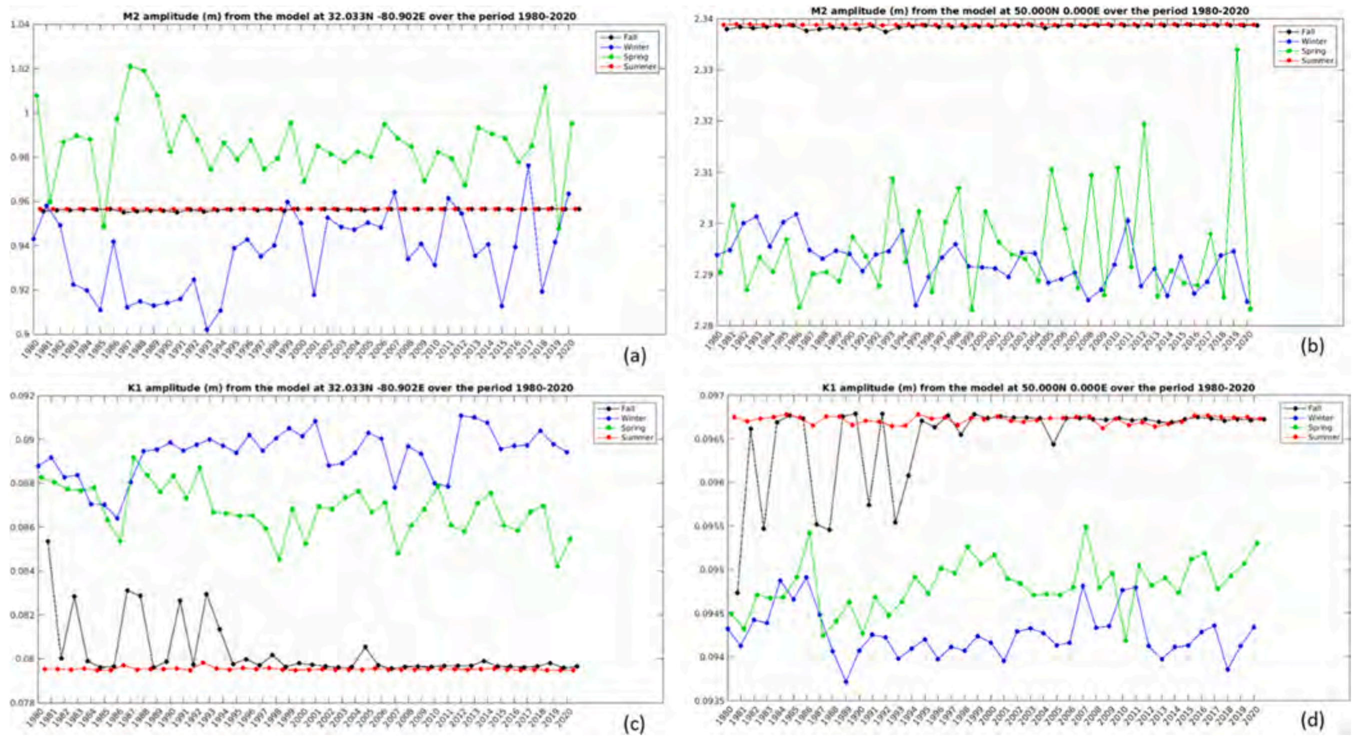

Fig. 12. Seasonal time series of the M2 (a and b) and K1 (c and d) tidal amplitudes (in m) from the global model, at points located along the coast of Georgia, US (a and c) and in the English Channel, off France (b and d).

The variability is globally twice smaller for K1, and mainly concentrated in the Arctic Ocean (Baffin Bay, Canadian Archipelago), in the Mid-Atlantic Bight and in the Okhotsk Sea. As one could expect, the smallest variability occurs in Summer, when the sea ice cover is minimal in the Arctic Ocean. This result also highlights the lower impact of the Antarctic sea ice cover on the global tidal simulations, even during the Southern Winter season, as there are less open-sea continental shelves in the Southern Ocean. For the other seasons, and in particular Winter and Spring, some regions outside the Arctic Ocean clearly show variations at the centimetre level on M2, especially in the Atlantic Ocean, all along the US coast down to Florida, and along the European coast up to the English Channel. Variability patterns are also observed in Spring along the Nicaragua coast in the Caribbean Sea, as well as on the Amazon shelf. Bij de Vaate et al. (2021) also showed that the Arctic land-fast ice impacts the seasonal modulation of M2 in these regions. Such patterns are consistent with the strong energetic connection that exists between the Hudson Bay/Foxe Basin area and the North Atlantic Ocean, in terms of tidal energy fluxes. The sea-ice impact outside the Arctic Ocean appears to be amplified in regions of tidal resonance, such as the European continental shelf. For K1, the impact outside the Arctic Ocean is much smaller (note that the scale is not the same as for the M2 maps), but one can clearly see the difference in variability in the Baffin Bay and in the Okhotsk Sea, depending on the season. It should be noted that the sea ice concentration maps include the Okhotsk Sea, which explains the large variability in this region.

The seasonal time series of the M2 and K1 amplitudes from the model are shown in Fig. 12 at two points, the first one along the US East coast, off Georgia, and the second one in the English Channel, off Normandy, in France. In both cases, the M2 amplitudes vary of several centimetres from one year to the next, and from one season to the other. However, although tide gauge observations (not shown here) show similar ranges of M2 variability, it is difficult to find a correlation between the time series of in situ data and from the model. Again, other processes than the variations in the sea ice cover may impact the tidal amplitudes at the tide gauges, which are not considered in our model simulations. Further analyses with in situ data are necessary, at larger scale like Bij de Vaate et al. (2021), to better understand the long-distance effect of the Arctic sea ice cover on the seasonal tides in the global ocean. Given the scale of the modelled tidal variability, and the associated uncertainties, it appears difficult to estimate the impact of the sea-ice cover decay in the Arctic over the years without considering more tide gauge stations (still, the difficulty remains to find long time series of hourly observations covering the 1980–2020 period).

4. Discussion and conclusion

Investigations about the tidal variability associated with the sea ice cover variability, both from in situ records or through numerical simulations, remain a complex and uncertain challenge. The different variability time scales (seasonal, inter-annual, long term) driving the sea-ice cover and its impact on tidal variability mix up, with more or less comparable amplitudes. Changes observed in the tidal estimates from in situ records may also be due to other ocean processes than variations in the sea ice cover, and there is no easy way to discriminate the causes, given that some of these effects can be produced by long-distance causes. It is difficult to deliver a general conclusion about this study, as the tidal response to sea ice changes is far from uniform in space, and may differ when considering the M2 or K1 tides. Let just state that the seasonal tidal variability is the dominant one, the inter-annual variability comes second and that long-term tidal variability, when detectable, remains the weakest one. By nature, the tidal spatial scales, which range between a few kilometres to thousands of kilometres, also make it difficult to assess the impact of the long-term/inter-annual/seasonal sea-ice cover variability in the Arctic Ocean, as some effects can be very local, and other may occur at long distances, as can be observed at the ice-free Norwegian in situ stations, or outside the Arctic Ocean, with the global simulations.

Improving knowledge about the interconnections between sea ice cover and tidal variability at these various time scales is of particularly high relevance to improve tidal corrections for satellite altimetry observations no only in the Arctic Ocean, but also in the global ocean. Indeed, our analyses of the in situ observations and model simulations show that the tidal estimates can locally vary by several centimetres depending on the seasons and the years, even at very long distance, outside the Arctic Ocean. Today, satellite altimetry observations are corrected with sea-ice-free tidal models, which means that these tidal temporal variations linked to the sea ice are part of the uncertainty budget of these measurements. Our study shows that the uncertainties associated with the absence of sea ice in these tidal corrections can reach several centimetres not only in regions of the Arctic Ocean (Hudson Bay, Canadian Archipelago), but also in regions located at a long distance, such as the US Atlantic coast, the Gulf of Mexico, the North East Atlantic shelf, and the English Channel. Exploring ways of improvements of tidal models in this field is thus crucial to obtain better observational datasets worldwide and to better understand the ocean dynamics in the complex Arctic region.

In general, our regional simulations reproduce large scale effects, related to the energy budget and connections between basins. However, they generally do not represent well the local effects that may be more related to sea-ice thickness (and age) in shallow waters, which is not taken into account in the model today (only the sea-ice concentration has been considered for now).

Another important aspect that can have an impact on the regional simulations is the location of the open-boundary conditions (OBC). Indeed, such conditions are generally imposed from a static global tidal model (no temporal variability) and if the limits of the regional model domain are too close to regions with tidal temporal variability, the OBC may be too constraining or even inject errors from the global model into the regional model. Further analyses could be done considering prescribing OBC based on global simulations varying in time with the sea-ice cover (seasonal simulations for example). Still, the regional approach is particularly interesting as it allows much higher resolution and local tuning, and more relevant comparisons with local in situ measurements, unlike the global approach.

It would also be interesting in the future to explore similar simulations with a higher resolution global configuration such as the new FES2022 model, to see if the comparison with in situ observations improves.

Further regional and global analyses could also take into account atmospheric forcing in the tidal simulations, to better represent the sea water elevation and motion, and their interactions with the sea ice. Ultimately, investigations could be done considering a 3D ocean model coupled with sea ice, which is far beyond the scope of the present study, which aimed at focusing on 2D tidal simulations. It may also help discriminate the various processes that can drive the changes in tidal amplitudes in the in situ observations, and better understand the specific role of the sea ice cover.

Finally, the lack of long time series of in situ data at high frequency (hourly) is a strong limitation to such studies in the Arctic Ocean. Satellite altimetry observations can provide complementary information, but they are representative of an average over a 10-year period, mainly thanks to the CryoSat-2 mission. The CRISTAL mission is expected to continue the time series and provide data for the next ten years. In such a context, models are extremely useful tools to fill gaps, but they need accurate observations to be validated, at least during the most recent period. Unfortunately, it seems the trend is not favourable in terms of in situ instrumentation in the Arctic Ocean, as many regions remain uncovered with recent observations, while research programs provided a lot of data in the 1970–1980s. With the continuous decay of the sea ice cover in the Arctic Ocean, and the intensification of navigation and maritime activities in the region, we may expect that more measurements will be available in the future, to ensure safety of operations in an environment that may become more accessible but remains a remote region with harsh environmental conditions.

CRediT authorship contribution statement

Mathilde Cancet: Writing – review & editing, Writing – original draft, Validation, Supervision, Methodology, Investigation, Formal analysis, Data curation. **Florent H. Lyard:** Methodology, Writing – review & editing, Writing – original draft, Supervision. **Ergane Fouchet:** Writing – review & editing, Writing – original draft, Investigation, Data curation.

Declaration of competing interest

The authors declare the following financial interests/personal relationships which may be considered as potential competing interests:

This work is part of the ARKTALAS Hoavva study funded by the European Space Agency under the Contract 4,000,127,401/19/NL/LF.

Appendix

We provide here the figures showing the seasonal times series of the amplitude of the M2 and K1 tides extracted from the model and analysed from the tide gauge data for stations that highlight a clear seasonal cycle for tides (Fig. 13–Fig. 16, stations indicated as red dots on Fig. 2). Fig. 17–Fig. 19 show stations with no clear seasonal cycle (black dots on Fig. 2). We do not show the model time series for these stations, as they do not highlight any seasonal nor inter-annual variability (the model time series are very close from to each other and completely flat). The figures show high heterogeneity in the results, as discussed in details in Section 3.3 of the paper.

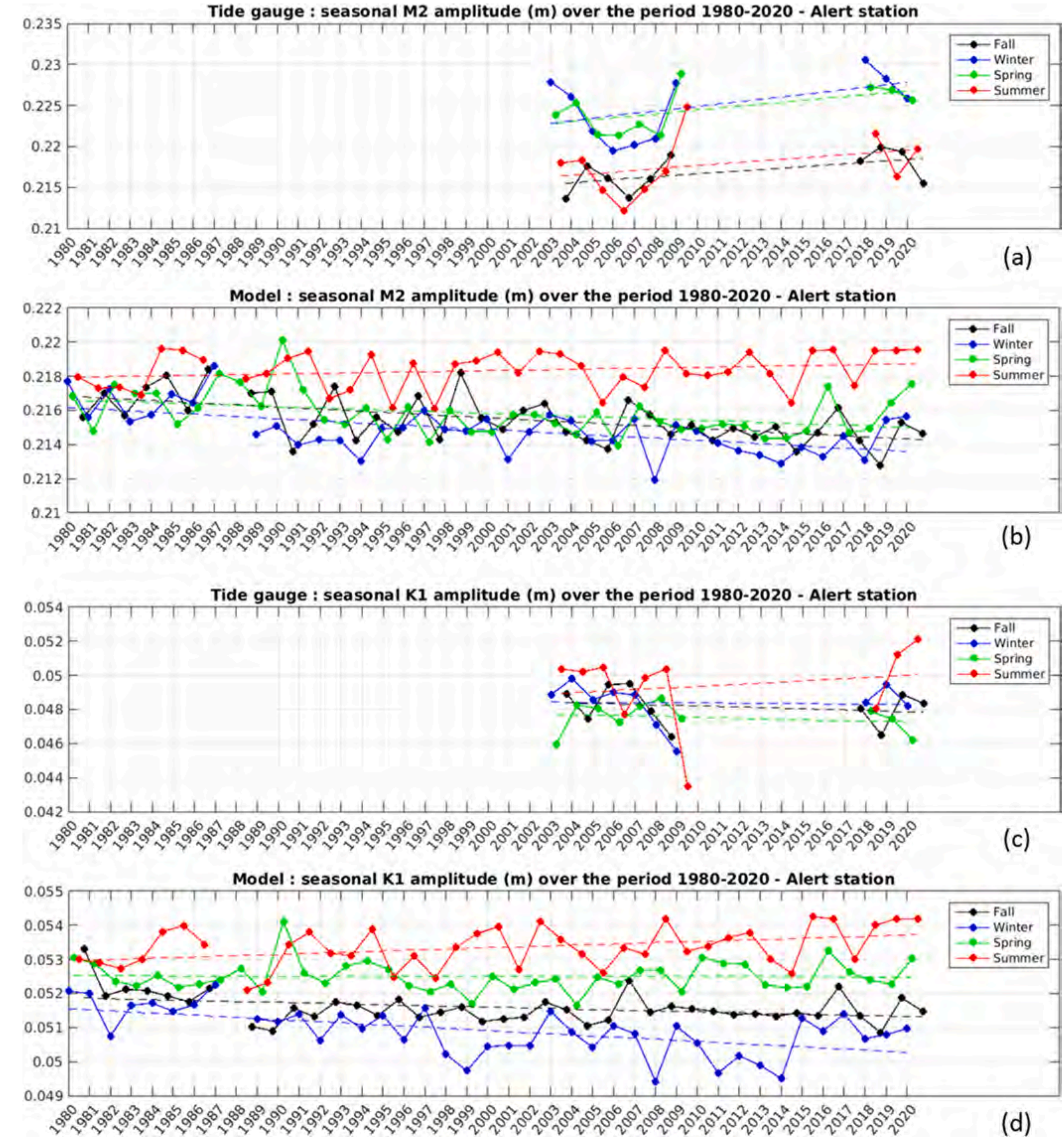

Fig. 13. Alert tide gauge: seasonal tidal amplitudes for the M2 (a and b) and K1 (c and d) tides from observations (a and c) and simulations (b and d) over the 1980–2020 time period. The coloured dashed lines show the linear trends of the time series.

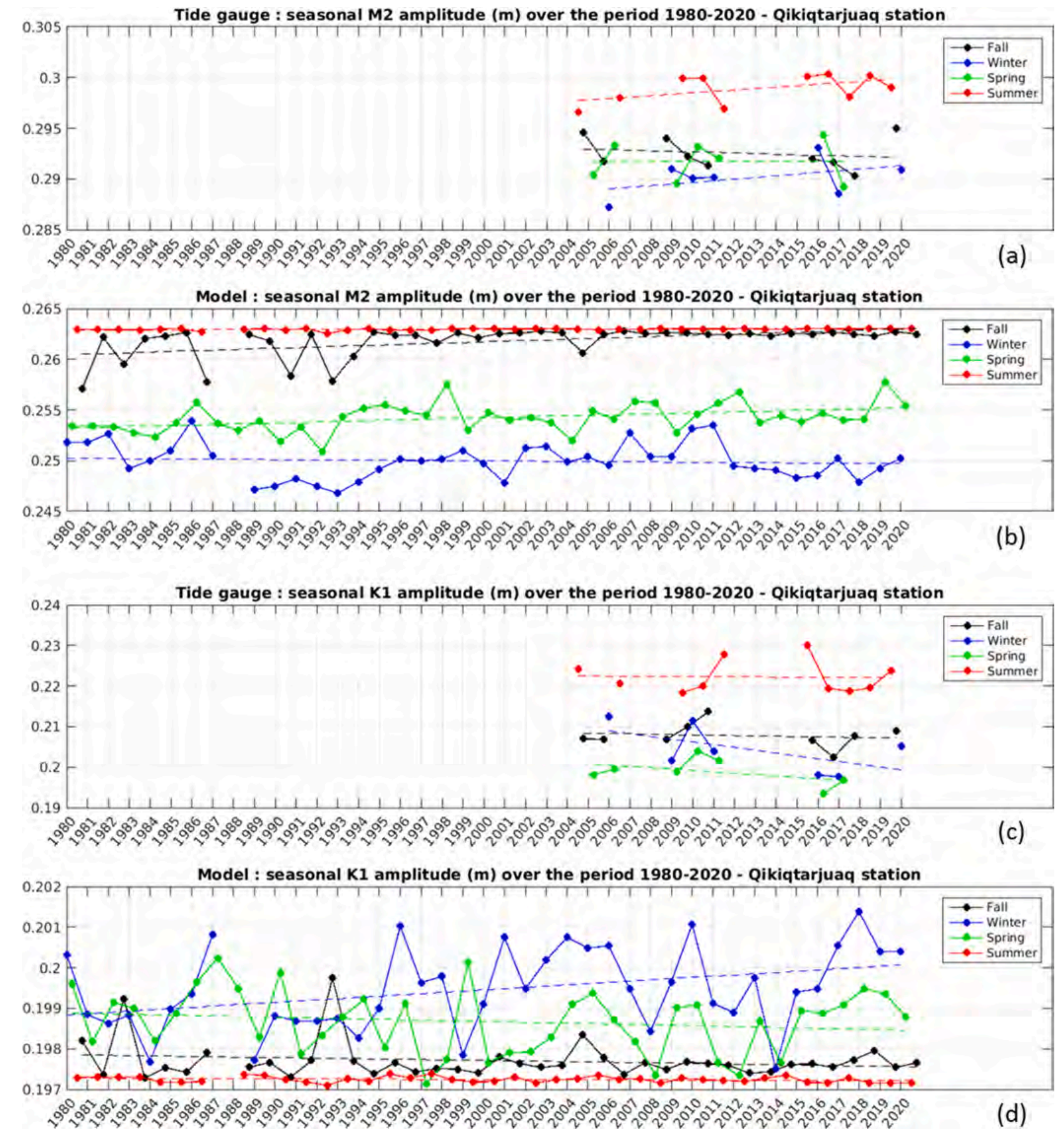

Fig. 14. Qikiqtarjuaq tide gauge: seasonal tidal amplitudes for the M2 (a and b) and K1 (c and d) tides from observations (a and c) and simulations (b and d) over the 1980–2020 time period. The coloured dashed lines show the linear trends of the time series.

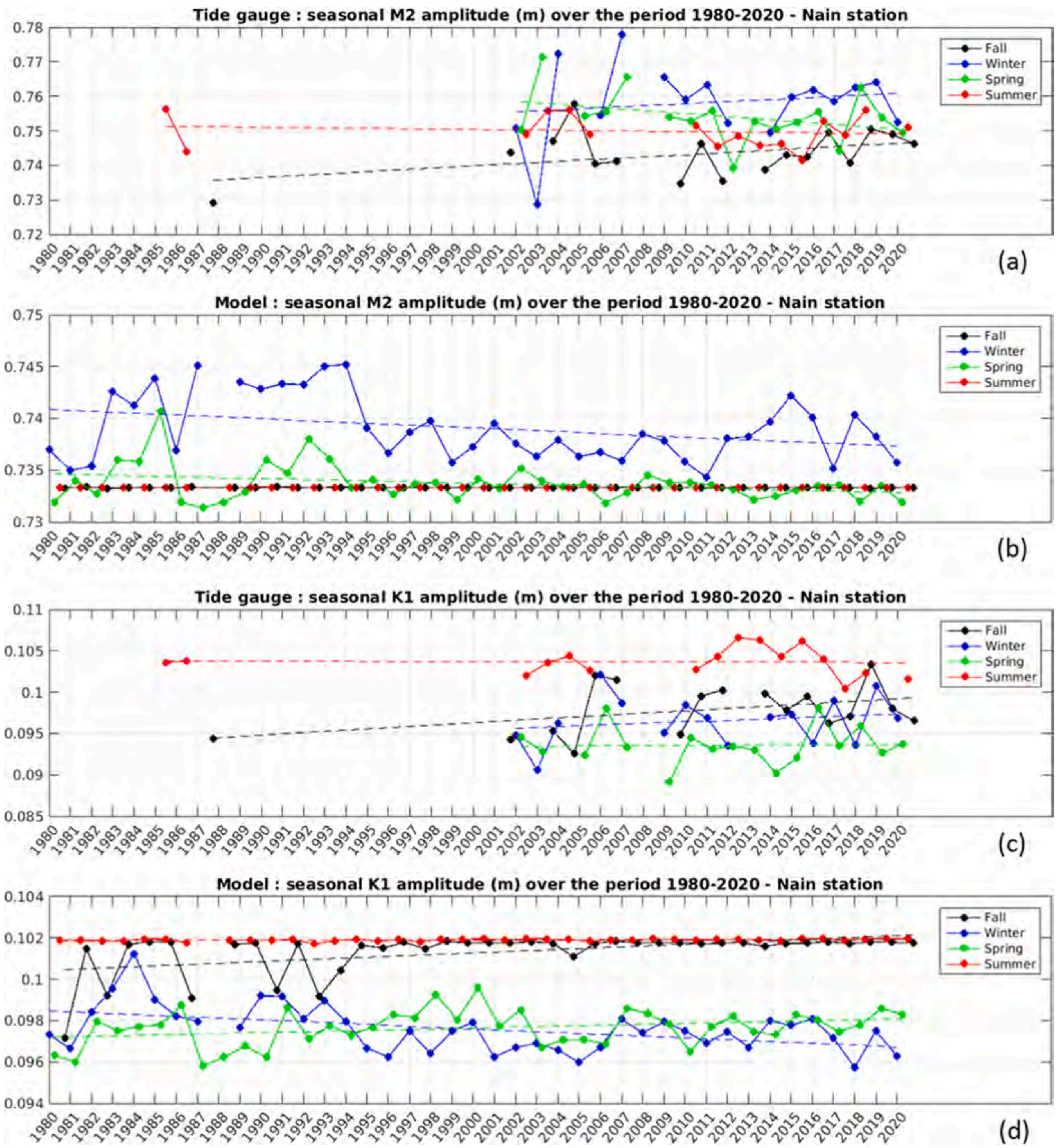

Fig. 15. Nain tide gauge: seasonal tidal amplitudes for the M2 (a and b) and K1 (c and d) tides from observations (a and c) and simulations (b and d) over the 1980–2020 time period. The coloured dashed lines show the linear trends of the time series.

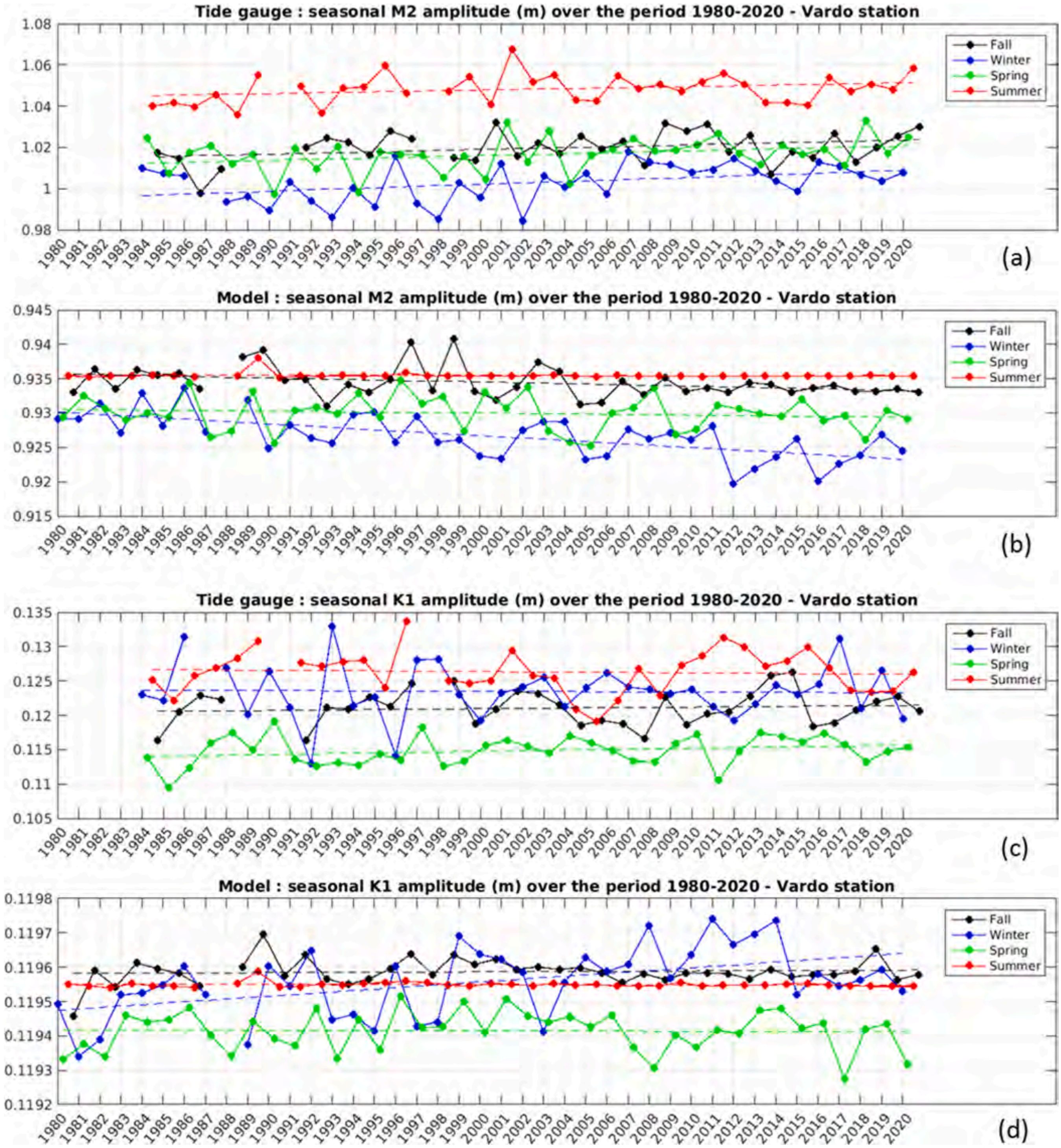

Fig. 16. Vardo tide gauge: seasonal tidal amplitudes for the M2 (a and b) and K1 (c and d) tides from observations (a and c) and simulations (b and d) over the 1980–2020 time period. The coloured dashed lines show the linear trends of the time series.

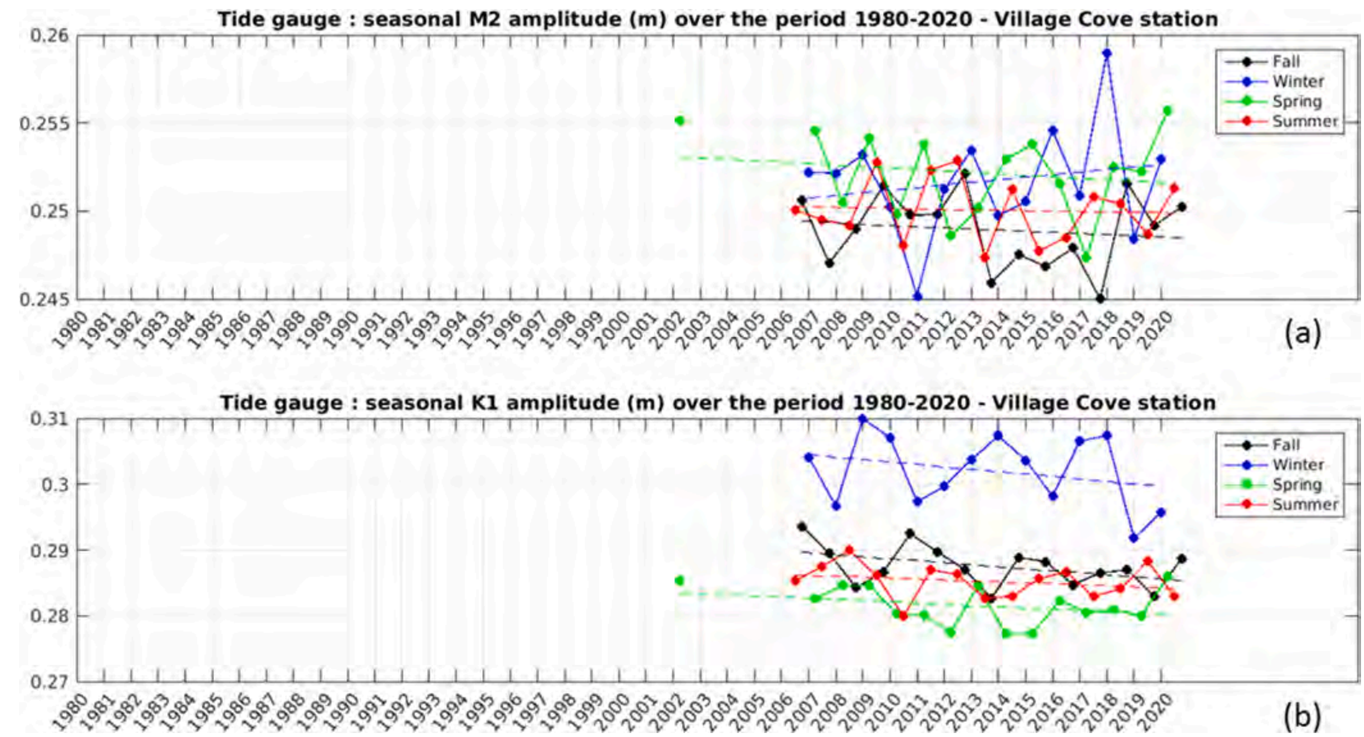

Fig. 17. Village Cove tide gauge: seasonal tidal amplitudes for the M2 (a) and K1 (b) tides from observations over the 1980–2020 time period. The coloured dashed lines show the linear trends of the time series.

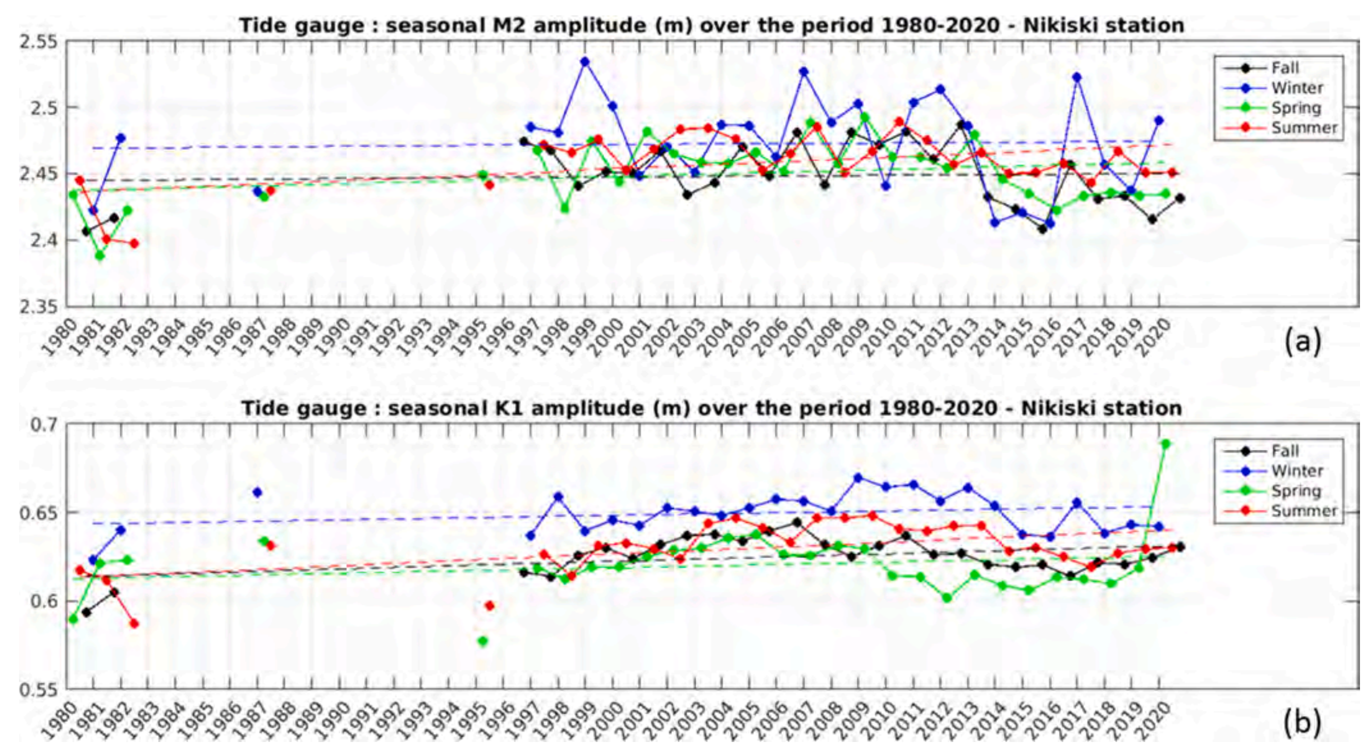

Fig. 18. Nikiski tide gauge: seasonal tidal amplitudes for M2 (a) and K1 (b) tides from observations over the 1980–2020 time period. The coloured dashed lines show the linear trends of the time series.

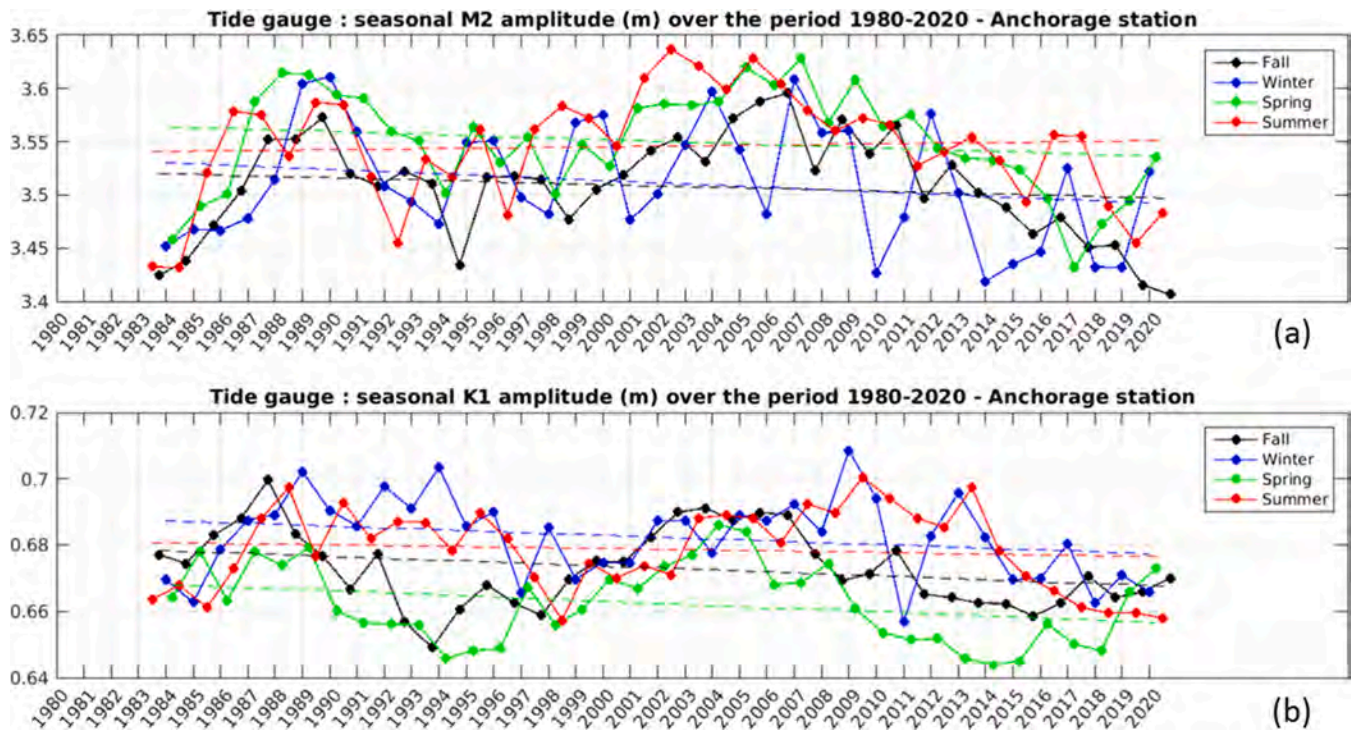

Fig. 19. Anchorage tide gauge: seasonal tidal amplitudes for the M2 (a) and K1 (b) tides from observations over the 1980–2020 time period. The coloured dashed lines show the linear trends of the time series.

Data availability

The authors do not have permission to share data.

References

Andersen, O.B., Rose, S.K., Hart-Davis, M.G., 2023. Polar ocean tides—Revisited using cryosat-2. Remote Sens 15, 4479. https://doi.org/10.3390/rs15184479.

Armitage, T.W.K., Bacon, S., Ridout, A.L., Thomas, S.F., Aksenov, Y., Wingham, D.J., 2016. Arctic sea surface height variability and change from satellite radar altimetry and GRACE, 2003–2014. J. Geophys. Res. Oceans. 121, 4303–4322. https://doi.org/10.1002/2015JC011579.

Bij de Vaat, I., Vasulkar, A.N., Slobbe, D.C., Verlaan, M., 2021. The influence of Arctic landfast ice on seasonal modulation of the M2 tide. J. Geophys. Res. 126, e2020JC016630. https://doi.org/10.1029/2020JC016630.

Caldwell, P.C., Merrifield, M.A., Thompson, P.R., 2015. Sea level measured by tide gauges from global oceans — The Joint Archive for Sea Level holdings (NCEI Accession 0019568), Version 5.5, NOAA National Centers for Environmental Information. Dataset. https://doi.org/10.7289/V5V40S7W.

Cancet, M., Andersen, O., Lyard, F., Cotton, D., Benveniste, J., 2018. Arctide2017, a high-resolution regional tidal model in the Arctic Ocean. Adv. Space Res. 62 (6), 1324–1343. https://doi.org/10.1016/j.asr.2018.01.007.

Carrère, L., Lyard F., Cancet, M., Allain D., Dabat, M.-L., Fouchet, E., Sahuc, E., Faugere, Y., Dibarboure, G., and Picot, N. (2022), A new barotropic tide model for global ocean: FES2022, presentation at the OSTST meeting 2022 in Venice, Italy, https://doi.org/10.24400/527896/a03-2022.3287.

Collins, A.K., Hannah, C.G., Greenberg, D., 2011. Validation of a high-resolution modelling system for tides in the Canadian Arctic Archipelago. Can. Tech. Rep. Hydrogr. Ocean Sci. 273 vii+72pp.

Comiso, J.C., 2012. Large decadal decline of the Arctic multiyear ice cover. J. Climate 25, 1176–1193. https://doi.org/10.1175/JCLI-D-11-00113.1.

Dunphy, M., Dupont, F., Hannah, C.G., Greenberg, D., 2005. Validation of a modelling system for tides in the Canadian Arctic Archipelago. Can. Tech. Rep. Hydrogr. Ocean Sci. 243 vi + 70 pp.

Godin, G., 1980. Modification of the tide in the Canadian Arctic by an ice cover, Manuscript Rep. Ser., 56. Dep. of Fish. Oceans, Ottawa, Ont., Canada.

Godin, G., 1986. Modification by an ice cover of the tide in James Bay and Hudson Bay. Arctic 39 (1), 65–67. March 1986.

Haigh, I., Marcos, M., Talke, S.A., Woodworth, P., Hunter, J., Haugh, B., Arns, A., Bradshaw, E., Thompson, P. (2021). GESLA Version 3: a major update to the global higher-frequency sea-level dataset. 10.31223/X5MP65.

Hannah, C., Dupont, F., Collins, A., Dunphy, M., Greenberg, D., 2008. Revisions to a modelling system for tides in the Canadian Arctic Archipelago. Can. Tech. Rep. Hydrogr. Ocean Sci. 259 vi+62pp.

Kagan, B.A., Sofina, E.V., 2010. Ice-induced seasonal variability of tidal constants in the Arctic Ocean. Cont. Shelf. Res. 30, 643–647. https://doi.org/10.1016/j.csr.2009.05.010.

Kleptsova, O., Pietrzak, J.D., 2018. High resolution tidal model of Canadian Arctic Archipelago, Baffin and Hudson Bay. Ocean. Model. (Oxf) 128, 15–47. https://doi.org/10.1016/j.ocemod.2018.06.001 pages.

Kowalik, Z., Proshutinsky, A.Y., 1994. The Arctic Ocean tides. In: Johannessen, O.M., Muench, R.D., Overland, J.E. (Eds.), The Polar Oceans and Their Role in Shaping the Global Environment. American Geophysical Union, Washington, D. C. https://doi.org/10.1029/GM085p0137.

Kulikov, M., Medvedev, I., Kondrin, A., 2018. Seasonal variability of tides in the Arctic Seas. Russ. J. Earth Sci 18, 5003. https://doi.org/10.2205/2018ES000633.

Kwok, R., 2018. Arctic sea ice thickness, volume, and multiyear ice coverage: losses and coupled variability (1958–2018). Environ. Res. Lett. 13, 105005. https://doi.org/10.1088/1748-9326/aae3ec.

Lyard, F., 1997. The tides in the Arctic Ocean from a finite element model. J. Geophys. Res. 102 (C7), 15611–15638. https://doi.org/10.1029/96JC02596.

Lyard, F.H., Allain, D.J., Cancet, M., Carrère, L., Picot, N., 2021. FES2014 global ocean tide atlas: design and performance. Ocean Sci. 17, 615–649. https://doi.org/10.5194/os-17-615-2021.

Lyard, F., Lefevre, F., Letellier, T., Francis, O., 2006. Modelling the global ocean tides: modern insights from FES2004. Ocean. Dyn. 56. https://doi.org/10.1007/s10236-006-0086-x.

Lynch, D.R., Gray, W.G., 1979. A wave equation model for finite element tidal computations. Comput. Fluids. 7, 207–228. https://doi.org/10.1016/0045-7930(79)90037-9.

Müller, M., Cherniawsky, J., Foreman, M., Storch, J.-S., 2014. Seasonal variation of the M2 tide. Ocean. Model. (Oxf). https://doi.org/10.1007/s10236-013-0679-0.

Morlighem, M., et al., 2017. BedMachine v3: complete bed topography and ocean bathymetry mapping of Greenland from multibeam echo sounding combined with mass conservation. GRL 44 (21), 11051–11061. https://doi.org/10.1002/2017GL074954.

Padman, L., Siegfried, M.R., 2018. Ocean tides affect ice loss from large polar ice sheets. Eos. (Washington. DC) 99. https://doi.org/10.1029/2018EO092835. Published on 20 February 2018.

Prandi, P., Ablain, M., Cazenave, A., Picot, N., 2012. A new estimation of mean sea level in the Arctic Ocean from satellite altimetry. Mar. Geod. 35, 61–81. https://doi.org/10.1080/01490419.2012.718222.

Ray, R., 2013. Precise comparisons of bottom-pressure and altimetric ocean tides. JGR, Oceans 118, 4570–4584. https://doi.org/10.1002/jgrc.20336. VOL.

Ray, R., 2016. On measurements of the tide at Churchill, Hudson Bay. Atmosphere-Ocean 54 (2), 108–116. https://doi.org/10.1080/07055900.2016.1139540.

Rippeth, T.P., Likncoln, B.J., Lenn, Y.-D., Mattias Green, J.A., Sundfjord, A., Bacon, S., 2015. 2015, Tide-mediated warming of arctic halocline by atlantic heat fluxes over rough topography. Nat. Geosci. 8, 191–194 volumepages.

Rotermund, L.M., Williams, W.J., Klymak, J.M., Wu, Y., Scharien, R.K., Haas, C., 2021. The effect of Sea ice on tidal propagation in the Kitikmeot Sea, Canadian Arctic Archipelago. J. Geophys. Res. 126 (5). https://doi.org/10.1029/2020JC016786 e2020JC016786.

Schaffer, J., Timmermann, R., Arndt, J.E., Rosier, S.H.R., Anker, P.G.D., Callard, S.L., Davis, P.E.D., Dorschel, B., Grob, H., Hattermann, T., Hofstede, C.M., Kanzow, T., Kappelsberger, M., Lloyd, J.M., Ó Cofaigh, C., Roberts, D.H., 2019. An update to Greenland and Antarctic ice sheet topography, cavity geometry, and global bathymetry (RTopo-2.0.4). PANGAEA. https://doi.org/10.1594/PANGAEA.905295. Supplement to: Schaffer, J. et al. (2020): Bathymetry constrains ocean heat supply to Greenland's largest glacier tongue. Nature Geoscience, 13(3), 227-231.

St-Laurent, P., Saucier, F.J., Dumais, J.-F., 2008. On the modification of tides in a seasonally ice-covered sea. J. Geophys. Res. 113, C11014. https://doi.org/10.1029/2007JC004614.